

A phosphorylation-deficient ribosomal protein eS6 is largely functional in *Arabidopsis thaliana*, rescuing mutant defects from global translation and gene expression to photosynthesis and growth

Anwasha Dasgupta¹  | Ricardo A. Urquidi Camacho²  | Ramya Enganti¹  |
 Sung Ki Cho¹  | Lindsey L. Tucker¹  | John S. Torreverde¹  |
 Paul E. Abraham^{2,3}  | Albrecht G. von Arnim^{1,2} 

¹Department of Biochemistry & Cellular and Molecular Biology, The University of Tennessee, Knoxville, Tennessee, USA

²Graduate School of Genome Science and Technology, The University of Tennessee, Knoxville, Tennessee, USA

³Biosciences Division, Oak Ridge National Laboratory, Oak Ridge, Tennessee, USA

Correspondence

Albrecht G. von Arnim, Department of Biochemistry & Cellular and Molecular Biology, The University of Tennessee, Knoxville, TN 37996-0840, USA.
 Email: vonarnim@utk.edu

Funding information

This work was supported by grants from the National Science Foundation (IOS-1456988 and MCB-1546402 to AGV) and the National Institutes of Health (NIH R15 GM129672 to AGV) and by the Donald L Akers Jr. Faculty Enrichment Fellowship to AGV.

Abstract

The eukaryote-specific ribosomal protein of the small subunit eS6 is phosphorylated through the target of rapamycin (TOR) kinase pathway. Although this phosphorylation event responds dynamically to environmental conditions and has been studied for over 50 years, its biochemical and physiological significance remains controversial and poorly understood. Here, we report data from *Arabidopsis thaliana*, which indicate that plants expressing only a phospho-deficient isoform of eS6 grow essentially normally under laboratory conditions. The eS6z (*RPS6A*) paralog of eS6 functionally rescued a double mutant in both *rps6a* and *rps6b* genes when expressed at approximately twice the wild-type dosage. A mutant isoform of eS6z lacking the major six phosphorylatable serine and threonine residues in its carboxyl-terminal tail also rescued the lethality, rosette growth, and polyribosome loading of the double mutant. This isoform also complemented many mutant phenotypes of *rps6* that were newly characterized here, including photosynthetic efficiency, and most of the gene expression defects that were measured by transcriptomics and proteomics. However, compared with plants rescued with a phospho-enabled version of eS6z, the phospho-deficient seedlings retained a mild pointed-leaf phenotype, root growth was reduced, and certain cell cycle-related mRNAs and ribosome biogenesis proteins were misexpressed. The residual defects of the phospho-deficient seedlings could be understood as an incomplete rescue of the *rps6* mutant defects. There was little or no evidence for gain-of-function defects. As previously published, the phospho-deficient eS6z also rescued the *rps6a* and *rps6b* single mutants; however, phosphorylation of the eS6y (*RPS6B*) paralog remained lower than predicted, further underscoring that

Anwasha Dasgupta, Ricardo A Urquidi Camacho, and Ramya Enganti made similar and substantial contributions and should be considered co-first-authors.

This is an open access article under the terms of the [Creative Commons Attribution-NonCommercial-NoDerivs](https://creativecommons.org/licenses/by-nc-nd/4.0/) License, which permits use and distribution in any medium, provided the original work is properly cited, the use is non-commercial and no modifications or adaptations are made.

© 2024 The Authors. *Plant Direct* published by American Society of Plant Biologists and the Society for Experimental Biology and John Wiley & Sons Ltd.



plants can tolerate phospho-deficiency of eS6 well. Our data also yield new insights into how plants cope with mutations in essential, duplicated ribosomal protein isoforms.

KEYWORDS

Arabidopsis, eS6, phosphorylation, polysome profiling, ribosome, translation

1 | INTRODUCTION

The function of ribosomes to assemble amino acids into proteins is conserved across the kingdoms of life. However, eukaryotic ribosomes contain expansion segments in their ribosomal RNAs, eukaryote-specific ribosomal proteins, and covalent modifications such as phosphorylation that are not found in prokaryotic ribosomes. Ribosomal protein 6 of the small 40S subunit (eS6 or RPS6) is a pan-eukaryotic protein and was the first ribosomal protein reported to be phosphorylated more than five decades ago (Gressner & Wool, 1974; Kabat, 1970). The amino-terminus of eS6 is buried in the 40S–60S subunit interface, whereas its carboxy-terminus ends in a long alpha helix that is located on the solvent-exposed side of the 40S and contains several serine and threonine residues that may be phosphorylated. The presence of phosphorylatable residues is highly conserved across eukaryotes even though the number of the residues varies among species.

Phosphorylation of eS6 is highly regulated. In animals, eS6 phosphorylation is sensitive to nutrients, hormones, growth factors, and a variety of stress conditions (Meyuhas, 2008). In plants, initial evidence for phosphorylation of eS6 came from tomato plants and maize root tips, where phosphorylation was suppressed by abiotic stresses, heat shock, and hypoxia, respectively (Bailey-Serres & Freeling, 1990; Scharf & Nover, 1982). In Arabidopsis, where up to seven sites can be phosphorylated, eS6 phosphorylation levels are induced in response to both internal and external signals such as light, the circadian clock, sucrose (Chen et al., 2018; Dobrenel et al., 2016; Enganti et al., 2018; Turkina et al., 2011), elevated CO₂ (Boex-Fontvieille et al., 2013), auxin (Schepetilnikov et al., 2013), and cytokinin (Yakovleva & Kulaeva, 1987). Several of these signals converge to regulate the level of phosphorylated eS6 (eS6-P) in a dynamic and elaborate manner. As a case in point, eS6-P is induced by daylight and repressed during a dark night. In contrast, under continuous light, that is, in the absence of a light-on signal to set the phase of the circadian clock, eS6-P is repressed by the circadian clock during the subjective day and induced during the subjective night (Choudhary et al., 2015; Enganti et al., 2018). Mathematical modeling of this seemingly contradictory signaling network has suggested that eS6-P may respond in a sensitive manner to subtle shifts in photoperiod or diel illumination (Panchy et al., 2020).

eS6 phosphorylation in plants is considered a canonical readout of the TOR–S6 kinase (TOR–S6K) pathway because this is the only established pathway known to regulate eS6 phosphorylation in plants (Chen et al., 2018; Dobrenel et al., 2016; Mahfouz

et al., 2006). Despite detailed insights into the regulation of eS6-phosphorylation by upstream signals and kinases, the biochemical and physiological role of eS6 phosphorylation states has remained fairly enigmatic. Phosphorylation of eS6 is observed in actively translating ribosomes (Duncan & McConkey, 1982). Knock-in mice expressing only the alanine-substituted, nonphosphorylatable version of eS6 exhibit severe whole-body phenotypes, including a reduced size, glucose intolerance, and muscle weakness, along with a higher rate of protein synthesis (Ruvinsky et al., 2005, 2009). In addition, the phosphorylation of mammalian eS6 is implicated in cell size control, hyperplasia in pancreatic cancer, glucose homeostasis, and activation of neurons (Khalaileh et al., 2013; Knight et al., 2012; Ruvinsky et al., 2005, 2009; Wittenberg et al., 2016). The consequences of eS6-P at the biochemical level including its effect on translation are not well understood. Mouse embryonic fibroblasts lacking phosphorylatable eS6 had decreased translation fidelity, an increased rate of translation overall, and proliferated faster (Wittenberg et al., 2016). Mammalian eS6-P was slightly more abundant on shorter coding sequences than long ones and was inferred to decline as ribosomes progressed along the mRNA, and eS6-P slightly boosted the translation efficiency of short mRNAs (Bohlen et al., 2021). eS6 phosphorylation has also been linked to transcriptional regulation of genes encoding mammalian ribosome biogenesis factors (Chauvin et al., 2014).

In budding yeast, a detailed study of eS6-P deficiency including ribosome footprinting did not discover any effect of the phosphorylation potential on bulk translation nor a role in the regulation of gene expression via transcription or translation. An effect on ribosome biogenesis was attributed to reduced protein expression (Yerlikaya et al., 2016). Recently, Arabidopsis eS6-phosphorylation was proposed to support translation re-initiation, based on differences between phospho-null and phospho-mimic versions with respect to (i) their *in vitro* interaction with the re-initiation supporting protein (RISP) and (ii) their ability to support the expression of a reinitiation-dependent reporter mRNA (Mancera-Martinez et al., 2021).

Here, we report our findings from an extensive characterization of plants lacking either one or both wild-type *RPS6* paralogs and harboring either wild-type or phospho-deficient eS6 transgenes. Paralog eS6z is encoded by the gene At4g31700 and used to be referred to as RPS6A and eS6A, and the second paralog, eS6y, is encoded by At5g10360 and is synonymous with RPS6B and eS6B. In Arabidopsis, the *RPS6A* and *RPS6B* genes are functionally largely equivalent but non-redundant (Creff et al., 2010). At least two functional alleles of



RPS6 are required for survival, but single *rps6a* and *rps6b* mutant plants are dwarfs. At least three alleles are required for wild-type growth. We find that a phospho-deficient allele of eS6 is able to rescue the lethality of plants lacking both wild-type *RPS6* genes. We also find it to be largely functional in complementing the growth defects in single-paralog mutants. Double *rps6a rps6b* mutants complemented with a P-deficient eS6 reverted to normal photosynthetic efficiency ($Q_{y_{max}}$) and had largely normal mRNA and protein levels for photosynthesis proteins. These P-deficient plants also had no striking defects in global translation, again complementing defects seen in the single *rps6* mutants. However, transcriptome analysis revealed that the plants displayed subtle defects in mRNA expression of several cytokinesis-related genes, and they overaccumulated ribosome biogenesis proteins. P-deficient plants also tended to have asymmetric cotyledons and transiently pointed first leaves, defects hinting at incomplete complementation of the *rps6* mutations and potentially indicating a whole-plant defect stemming from the P-deficiency. These results extend findings on the function of this conserved phosphorylation event from yeast and vertebrates to photosynthetic organisms.

2 | RESULTS

2.1 | A new allele for *rps6a* recapitulates the typical phenotypes of a previous null allele

In order to facilitate double mutant construction, we sought out a new insertion allele for the z paralog of eS6 (protein: eS6z; gene: *RPS6A*). The new null allele of *RPS6A*, *rps6a-2*, was marked by sulfadiazine resistance rather than kanamycin resistance (see Section 4, Figure S1A,B,C) and did not express detectable mRNA (Figure S1D). The *rps6a-2* allele recapitulated the phenotype of an earlier allele, *rps6a-1* (Creff et al., 2010) with respect to pointed primary leaves, short roots, and reduced seed set (Figure S2A–E).

Because we were planning to test the function of eS6 phosphorylation using eS6z as a stand-in for both paralogs, we wanted to confirm whether the functions of eS6z and eS6y are equivalent and interchangeable, as shown by Creff et al. (2010). Indeed, the new *rps6a-2* allele was fully complemented by either the *RPS6A* or *RPS6B* gene (Figure S3A). However, the *rps6b-1* allele was largely, but not fully, complemented by either *RPS6A* or *RPS6B* (Figure S3B). In these experiments, the transgenes consisted of the native promoter and the native exon-intron structure. We surmise that the complementation in the *rps6b-1* background was incomplete because the residual truncated transcripts made from the *RPS6B* gene, as shown by RT-PCR (Figure S1D), may interfere with gene expression of the transgene. However, other explanations, for example, the presence of an additional mutation in the *rps6b* strain, cannot be ruled out. This was not analyzed further. Taken together, these results confirm that eS6z and eS6y are functionally equivalent. From this point forward, we will refer to the *rps6a-2* allele just as *rps6a* and *rps6b-1* as *rps6b*.

2.2 | Phosphorylation-deficient alleles of eS6z and eS6y and their subcellular localization

We generated an extensive series of site-directed mutant alleles for both *RPS6A* and *RPS6B*. To prevent phosphorylation in the C-termini of eS6z and eS6y, specific serine or threonine residues (Figure 1a) were changed to alanine ($\Delta S > A$ alleles). To create phospho-mimic alleles, S or T were changed to aspartate ($\Delta S > D$ alleles; Figure S1E). Out of the seven and five phosphorylatable sites in the C-terminus of eS6z and eS6y, respectively, S229 was left mostly unchanged because it is less often detected as phosphorylated (Enganti et al., 2018; Turkina et al., 2011; Williams et al., 2003) and because the main sites corresponding to S237 and S240 are phosphorylated first (Williams et al., 2003) and at higher levels (Mergner et al., 2020) than S229.

eS6 was tagged with enhanced YFP (EYFP) and expressed in *Nicotiana benthamiana*. We tagged the N-terminus because tagging the C-terminus was more likely to disrupt the phosphorylation at that site. Both the wild-type and a phospho-deficient allele, eS6z $^{\Delta 75 > A}$, accumulated strongly in the nucleus and especially in the nucleolus, as well as in the cytosol, as expected for ribosomal proteins (Figure S4A). The EYFP-tagged eS6z wild-type and eS6z $^{\Delta 75 > A}$ mutant proteins also appeared in structures resembling mini-nucleoli and other small granules, collectively referred to as nuclear punctae. eS6z $^{\Delta 75 > A}$ formed punctae more often than eS6z wild type (Figure S4B). eS6z $^{\Delta 75 > A}$ transformed cells also tended to have more than one nucleolus, but this trend was not statistically significant (Figure S4C). Taken together, the phosphorylation status did not affect the subcellular targeting of eS6 in a major way.

2.3 | Plants that are deficient for eS6-P have no apparent defects in global translation and ribosome biogenesis

We generated double *rps6a rps6b* mutants that harbored transgenes with variably phospho-deficient versions of eS6z and eS6y. The transgenes contained eS6z or eS6y in the native genomic context (promoter, introns, UTRs; see Section 4). The majority of the work was done with an allele where 5 serines and 1 threonine were replaced with alanine ($\Delta 6S > A$; Figure S1E), and a few experiments were done with a $\Delta 3S > D$ allele of eS6y. As controls, double mutants were complemented with the hemagglutinin- (HA-) tagged version of eS6z (eS6z^{WT-HA}) or with wild-type eS6y. The eS6z $^{\Delta 6S > A}$ complemented plants were indeed deficient for eS6-P for both S237 and S240 (Figure 1b) as established with phospho-specific antibodies against these commonly phosphorylated sites (Enganti et al., 2018).

RNA-Seq and proteomics experiments to be described below demonstrated that the eS6z $^{\Delta 6S > A}$ mRNA and protein were expressed at an elevated level, equivalent to about 1.3- and 1.6-fold, respectively, of the native eS6z (Figure 1c). Therefore, it appears that the homozygous eS6z $^{\Delta 6S > A}$ transgene provides about as much eS6 mRNA and protein as can be expected in a heterozygous *rps6b* mutant, which is a recessive mutation with wild-type phenotype.

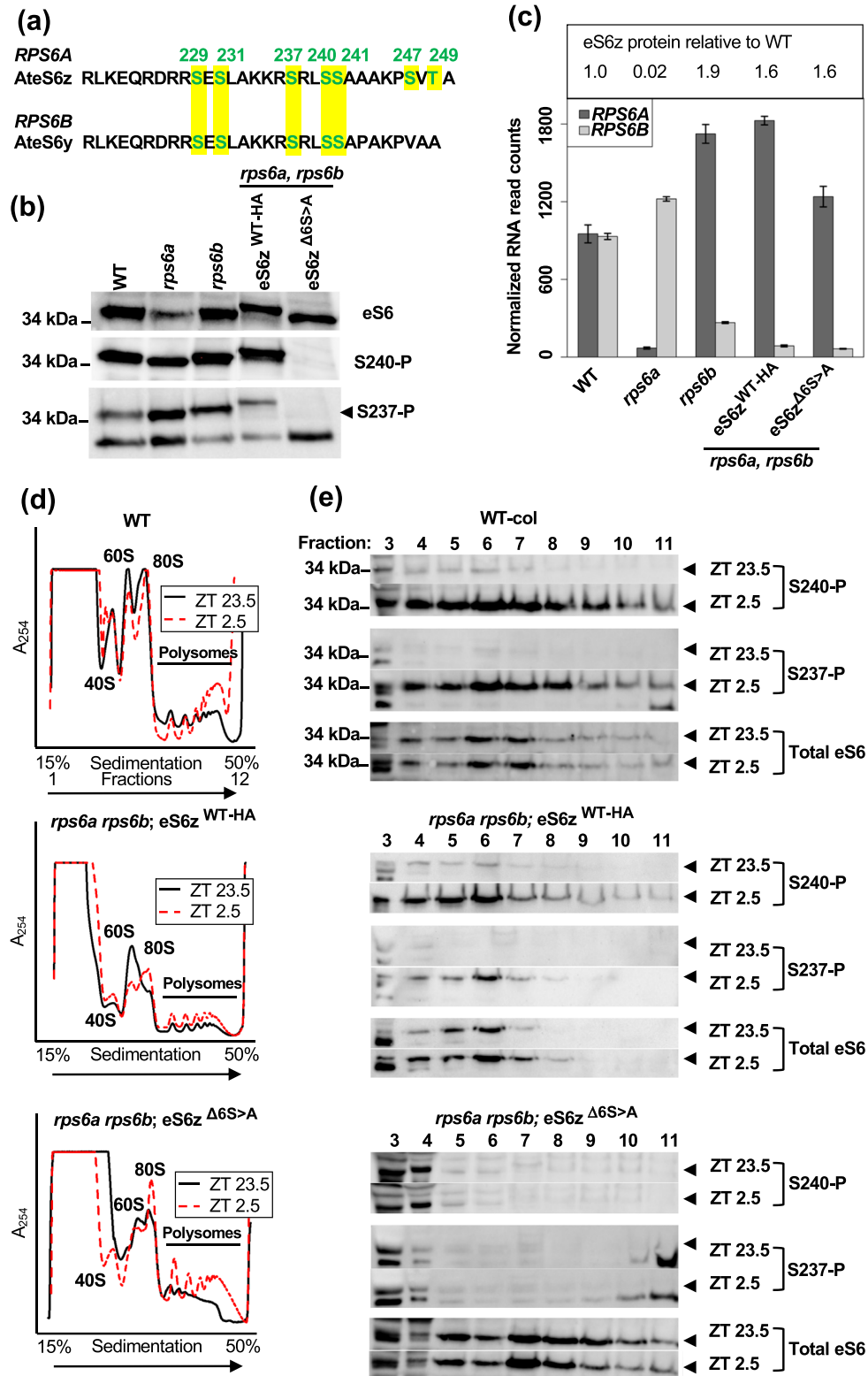


FIGURE 1 Legend on next page.



FIGURE 1 Biochemical characterization of plants lacking eS6 phosphorylation. (a) Phosphorylatable serines and one threonine in the C-termini of eS6z and eS6y. The mutated amino acids are S231, S237, S240 for the $\Delta 3S$ series; S231, S237, S240, S247, T249 for the $\Delta 5S$ mutant; and S231, S237, S240, S241, S247, T249 for the $\Delta 6S$ mutant. The wild-type eS6z is encoded by the *RPS6A* gene. One transgene expresses eS6z in a hemagglutinin-tagged form (WT-HA). eS6y is encoded by the *RPS6B* gene. A transgene for eS6y lacks an epitope tag (WT). (b) Phosphorylation of eS6 is not detected in *rps6a rps6b* double mutants that harbor the phospho-deficient eS6z $^{\Delta 6S > A}$ transgene. Whole-cell extracts from seedlings were probed on western blots with phospho-specific antibody for S240-P or S237-P and for total eS6 with an eS6 antibody (Enganti et al., 2018). Note: Our S237-P antibody detects two bands consistently. Repeated results and experience with the eS6z $^{\Delta 6S > A}$ allele have convinced us that the upper band running at ~ 35 kDa is the eS6 band. (b) mRNA read counts for eS6z and eS6y from an RNA-Seq experiment with the indicated genotypes. Proteomics data from the same genotypes expressed as a \log_2 -fold difference to wild type. Note that the two eS6z transgenes provide elevated levels of eS6 protein, as expected given the elevated mRNA read counts. (d) Polysome loading in *rps6a rps6b* double mutants complemented with phospho-enabled (eS6z $^{WT-HA}$) and phospho-deficient (eS6z $^{\Delta 6S > A}$) transgenes. Polysome loading was examined 30 min prior to lights-on (ZT23.5) and 2.5 h after lights-on (ZT2.5). Wild type is shown as a control. Representative polysome profiles show that eS6-P deficient plants are able to increase their ribosome loading during the dark-to-light shift. For quantitation, see Figure 3a. (e) Gradient fractions 3–11 from gradients in (d) were probed for phosphorylated S240 (S240-P) by immunoblotting. eS6 is phosphorylated in a polysome context in a light-inducible manner in double *rps6a rps6b* mutants complemented by an HA-tagged eS6z (middle) as well as wild type (top). In contrast, in the phospho-deficient plants (bottom), no light-inducible phosphorylation is detected at the position corresponding to eS6 (arrowhead). Note that fractions 3–4 at the top of the gradient contain several crossreacting proteins, which in the case of S237-P also appeared at the bottom of the gradient.

Light exposure induces a large and rapid increase in mRNA ribosome loading (Liu et al., 2012). To bring out the full scale of this shift, seedlings were grown in the absence of sucrose for our next experiments. Profiles were collected both .5 h before and 2.5 h after the daily dark-to-light shift (i.e., at zeitgeber times ZT23.5 and ZT2.5). For wild-type seedlings, polysomal eS6 phosphorylation at S240 and S237 increased robustly within 2.5 h of light exposure (Figure 1e), as expected (Enganti et al., 2018), along with an increase in global polysome loading (Figure 1d). A similar pattern was observed for double mutant seedlings harboring HA-tagged WT-eS6z. Both of these results confirm that phosphorylated eS6 gets incorporated into actively translating polysomes. The *rps6a rps6b* double mutants that were complemented with the phospho-deficient eS6z $^{\Delta 6S > A}$ transgene showed essentially normal polysome loading before and after the dark-to-light shift (Figure 1d; quantified in Figure 2a). S240 and S237 lacked phosphorylation, as expected, and total eS6 was still detected in polysomal fractions (Figure 1e). These data demonstrate that the eS6z $^{\Delta 6S > A}$ protein, despite lacking six major sites of phosphorylation, is incorporated into functional polysomes and supports global translation. Similar results were obtained when the double mutants were complemented with eS6y, or the phospho-mimic allele eS6y $^{\Delta 3S > D}$ (Figure 2c). In the experiments with eS6y as well as other experiments with *rps6* single mutants described below the polysome loading was higher across the board than in the double mutants complemented with eS6z $^{\Delta 6S > A}$. We attribute this to differences in plant growth or centrifugation conditions, as these data series were collected by different coauthors. In summary, eS6 protein functions normally in supporting global polyribosome loading despite being unphosphorylated ($\Delta 6S > A$) or harboring bona fide phospho-mimic mutations ($\Delta 3S > D$).

In order to discern any subtle effects of the phospho-deficiencies in eS6 on the translation apparatus, we thoroughly analyzed the translation apparatus of the *rps6a* and *rps6b* strains by polysome profiling with sucrose density gradient centrifugation. We detected an increase in the relative abundance of the 60S ribosomal subunit, which had

been suggested previously (Creff et al., 2010) and was statistically significant for both *rps6a* and *rps6b* in the light (Figure 2e–f, quantified in Figure S5).

Polysomes were decreased slightly in both *rps6a* and *rps6b*. In response to the dark-to-light shift, the fold-increase in polysomes (P/[NP + P]) was 1.53 or greater for both *rps6* mutants (Figures 2e–f and S5), showing that both *rps6* mutants responded as robustly as WT to the dark-to-light shift. From these data, we surmise that, because only a single paralog is available for eS6, the production of sufficient 40S ribosomal subunits is rate limiting in the *rps6* single mutants, not only for plant growth but also for ribosome production. Meanwhile, the 60S subunits overaccumulate, resulting in an imbalance between 40S and 60S in both *rps6* mutants as compared with wild type. When *rps6a rps6b* were complemented with phospho-deficient eS6z $^{\Delta 6S > A}$, the accumulation of the 60S ribosomal subunit was not elevated over wild type (Figure 2b) and this was also the case for the eS6y 3S > D mutant (Figure 2d). These results indicate that the phospho-deficient and phospho-mimic isoforms of eS6 can function adequately in ribosome biogenesis.

We note here that eS6 was phosphorylated normally in both the *rps6a* and *rps6b* single mutants. At the end of night, the phosphorylation of S237 and S240 was low overall and almost absent in polysomes. It increased dramatically, overall as well as in polysomes, with the dark-to-light shift (Figure 2e–f). These results match those in wild type (Enganti et al., 2018) and show that both eS6z and eS6y are phosphorylated under light conditions in a polysome context and that both isoforms are recognized by phospho-specific antibodies to both S237 and S240.

2.4 | Plants that are deficient for eS6-P grow largely normally

Considering that *rps6a rps6b* double mutants are embryo-lethal (Creff et al., 2010), it was striking that the P-deficient plants harboring only

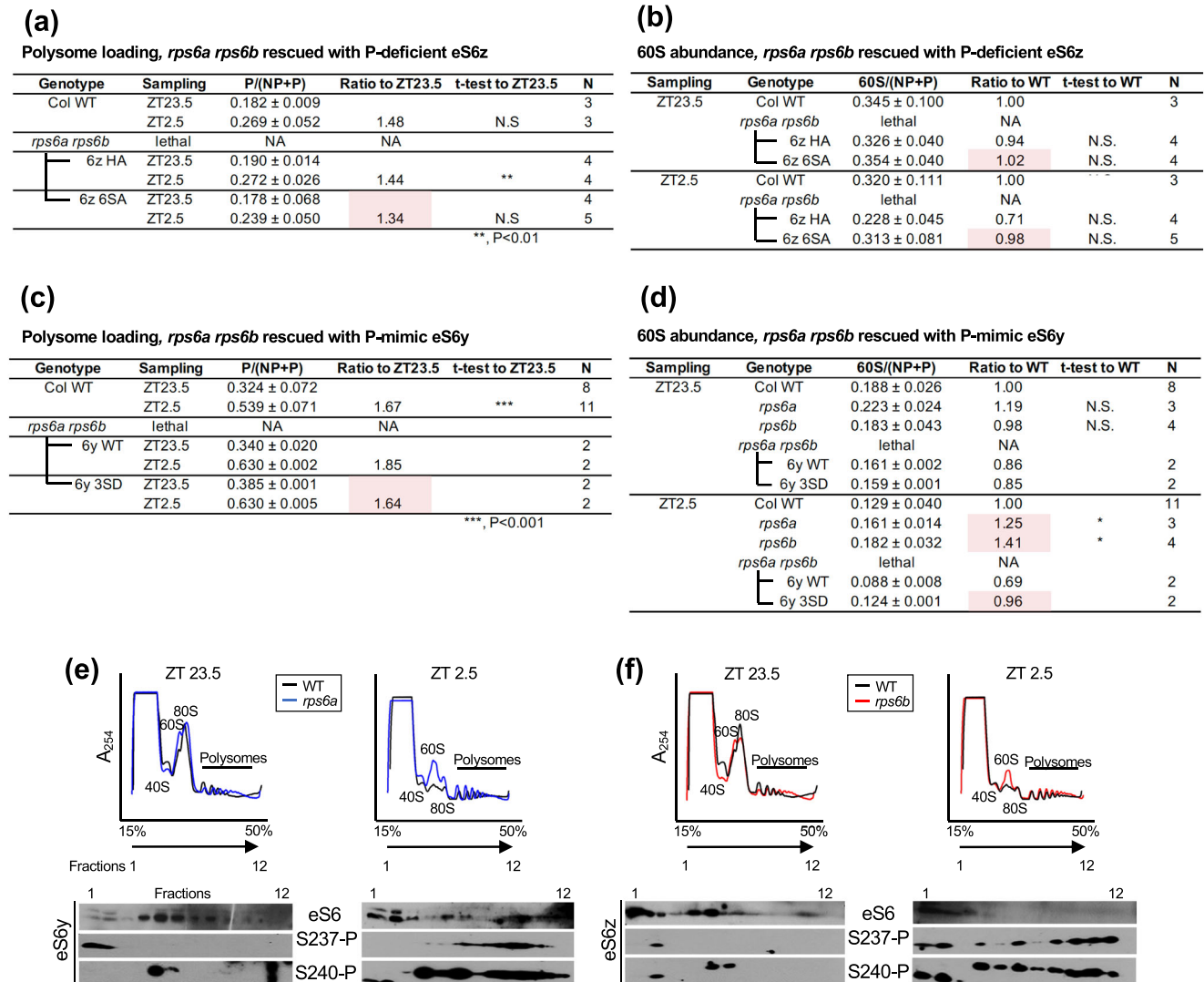
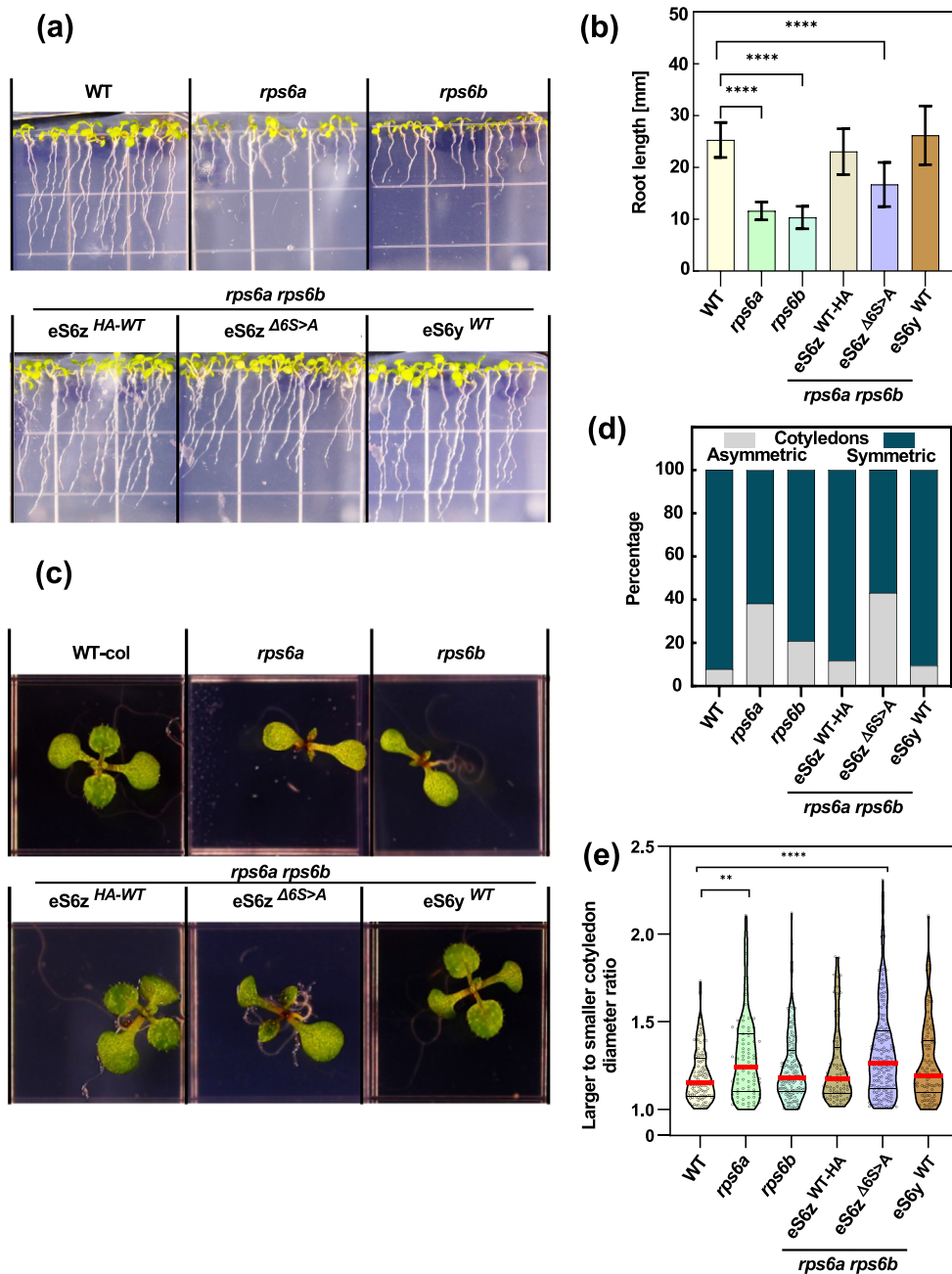


FIGURE 2 The phospho-deficient eS6z effectively rescues global polysome loading in the *rps6a rps6b* double mutant. Summary of polysome profiles of *rps6a rps6b* double mutant seedlings complemented with various P-enabled and P-deficient eS6 isoforms. N indicates the number of replicate gradients. (a, b) Complementation of double mutants with alleles of eS6z. A wild-type allele and the eS6z^{Δ65>A} phospho-deficient allele were used. In the 6A^{Δ65>A} line, all eS6 is phospho-deficient. (a) Fraction of RNA in polysomes P/(NP + P), focusing on the dark-to-light shift between ZT23.5 (30 min before lights-on) and ZT2.5 (150 min after lights on). (b) Fraction of RNA in the free 60S ribosomal subunit peak, which is often elevated in *rps6a* and *rps6b* single mutants, consistent with a 40S biogenesis defect. (c, d) Complementation of double mutants with alleles of eS6y. A wild-type allele and a phospho-mimic allele were used. The data for WT are from Figure S5. (c) Fraction of RNA in polysomes P/(NP + P). (d) Fraction of RNA in the free 60S ribosomal subunit peak. (e, f) Polyribosome profiles in single *rps6* mutants demonstrate an imbalance in 40S and 60S subunits. (e) Polyribosome profiles of *rps6a* versus wild-type seedlings at ZT23.5 (30 min before lights-on) and at ZT2.5 (150 min after lights-on). The immunoblots in *rps6a* mutants show the light-stimulated phosphorylation status of eS6y using two phospho-specific antibodies against P-S237 and P-S240 as well as total eS6. (f) Same as (e) for *rps6b* mutant seedlings. The protein detected on immunoblots is eS6z.

eS6z^{Δ65>A} were fully viable. This shows that phosphorylation is not necessary for functional ribosomes. However, a number of subtle growth defects were observed. First, root growth was reduced in a repeatedly selfed, homozygous, phospho-deficient line (Figure 3a,b) as compared with phospho-enabled eS6z^{WT-HA} and wild-type eS6y. Second, young eS6z^{Δ65>A} complemented seedlings had pointed first leaves (Figure 3c), a common phenotype in ribosomal protein mutants, including *rps6a* and *rps6b*. The pointed leaf phenotype is not due to the fact that eS6y is missing because *rps6a rps6b* heterozygotes

(which contain ~50% each of eS6z and eS6y) also have the pointed leaf phenotype (Creff et al., 2010; Ren et al., 2012), and eS6z^{WT-HA} plants did not have pointed leaves (Figure 3c). Third, we newly observed that *rps6a* mutants, and to a lesser degree *rps6b* as well, tend to have cotyledons that differ in size. This asymmetry was retained in the eS6z^{Δ65>A} seedlings (Figure 3c-e). The phenotypic observations suggest that eS6 phosphorylation is not directly affecting all translation, but may be more subtle, affecting only some transcripts, growth stages, and/or tissue types.

FIGURE 3 Plants that are deficient for eS6-P grow largely normally with exceptions during seedling establishment. (a) Phenotype of 11-day-old *rps6a rps6b* double mutant seedlings complemented with a phospho-deficient version of eS6z, as compared with controls complemented with phospho-enabled eS6z^{WT-HA} or with wild-type eS6y. Single *rps6a* and *rps6b* mutants are shown for reference as double *rps6a rps6b* mutants are lethal. Seedlings were germinated and grown on vertical agar-solidified MS salt medium. (b) Root lengths of seedlings from experiment (a). Error bars indicate standard deviations, and **** indicates $p < .0001$ by Welch's *t*-test. (c) Pointed-leaf and asymmetric cotyledon phenotypes in 7-day-old seedlings of phospho-deficient *rps6a rps6b* double mutants. This phenotype is characteristic of *rps6a* and *rps6b* single mutants but is not observed in controls with phospho-enabled eS6. (d) Cumulative histogram and (e) violin plot of the asymmetric cotyledon phenotype. Medians are indicated by red bars. ** $p = .0056$ and **** $p < .0001$ by Mann-Whitney test.



To characterize the phospho-deficient plants in more detail, we measured the photosynthetic efficiency of photosystem II ($Q_{y_{max}}$). In keeping with the misexpression of photosynthesis genes in *rps6a* mutant seedlings (see RNA-Seq experiment below), photosystem II efficiency was reduced in *rps6a* and *rps6b* mutants in seedlings (Figure 4a–b) and in rosette-stage plants grown at 22°C or at 12°C (Figure 4c–d). The phospho-deficient plants (*rps6a rps6b*; eS6z^{Δ6S>A}) were largely rescued for photosynthetic efficiency at all stages.

2.5 | Gene expression defects in seedlings lacking eS6-phosphorylation

The transcriptome of *rps6a rps6b*; eS6z^{Δ6S>A} phospho-deficient seedlings was analyzed in triplicate by RNA-sequencing alongside

eS6z^{WT-HA} complemented plants, *rps6a* and *rps6b* mutants, and wild type. Mapping the reads originating from the *RPS6* genes confirmed that the eS6z^{Δ6S>A} plants indeed only contained phospho-deficient eS6 (Figure S6).

Principal component analysis (PCA) revealed that the three biological replicates clustered closely together, whereas the five genotypes were distinct. *rps6a* and *rps6b* were clearly distinct from WT in PC1 and also differed from each other in PC2 (Figure 5a). Filtering for differentially expressed genes between WT and the mutants and complementation lines confirmed that eS6z^{WT-HA} and eS6z^{Δ6S>A} transgenes substantially complemented the *rps6a rps6b* double mutation (Figure 5c). Of 93 mRNAs that were differentially expressed at a false discovery rate (FDR) $< .05$ between eS6z^{WT-HA} and WT, only 15 differed by >2 -fold. The phospho-deficient eS6z^{Δ6S>A} transgene complemented the double-*rps6* phenotype slightly less well than the

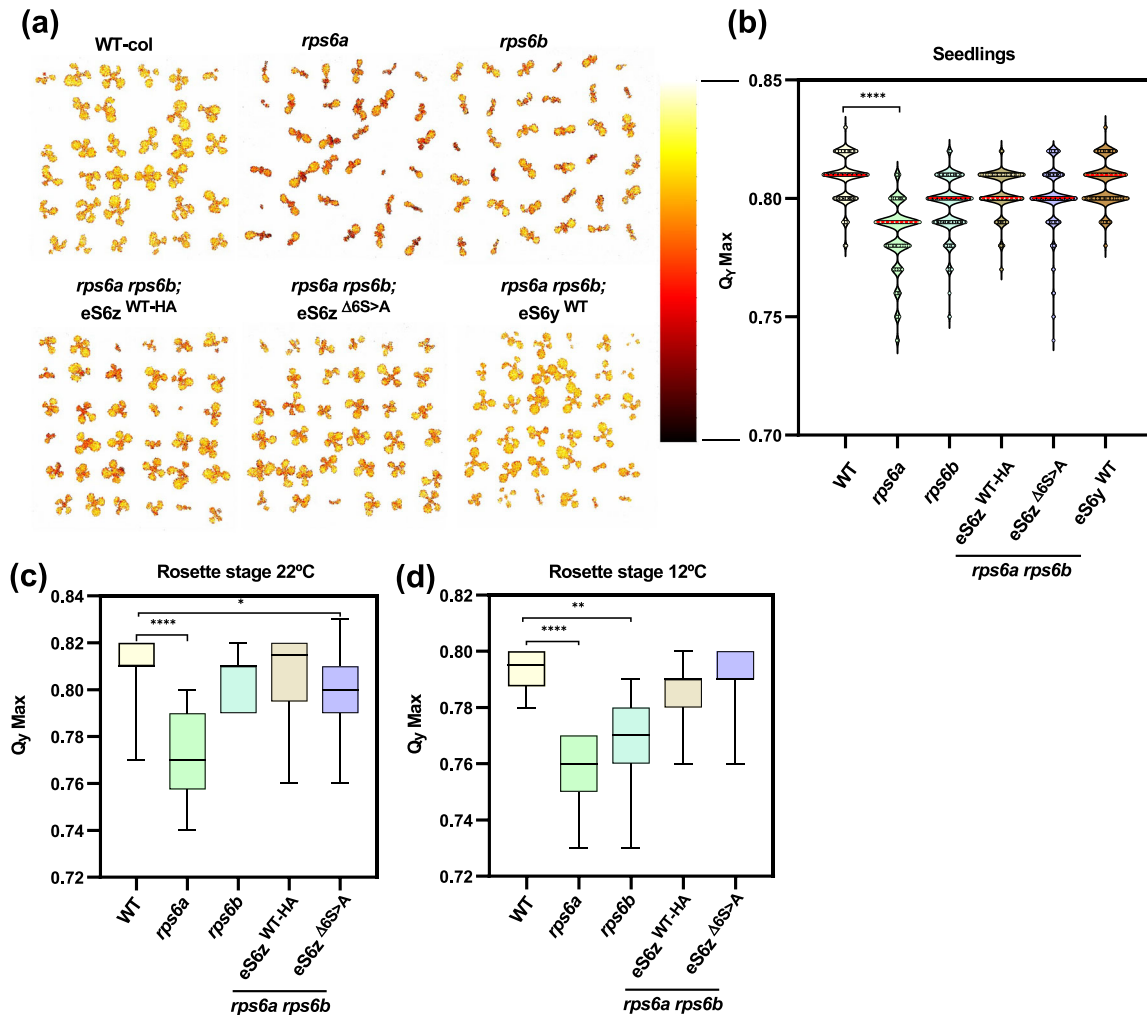


FIGURE 4 Photosynthetic efficiency in seedlings and mature rosettes of phospho-deficient and phospho-enabled *rps6a rps6b* double mutants. $Q_{y \text{ max}}$ measures the quantum efficiency of photosystem II. (a) $Q_{y \text{ max}}$ heatmaps in 11-day-old seedlings complemented with phospho-enabled (eS6z^{WT-HA} and eS6y^{WT}) and phospho-deficient (eS6z ^{$\Delta 6S > A$}) transgenes. *Rps6a* and *rps6b* single mutants are shown for comparison, with *rps6a* showing a stronger photosynthetic defect than *rps6b*. (b) Violin plots to quantify data from experiments such as panel (a). Medians are indicated by red bars. **** indicates $p < .0001$ by Mann-Whitney test. (c, d) $Q_{y \text{ max}}$ in the leaves of 3-week-old rosettes for the indicated genotypes of phospho-deficient plants (eS6z ^{$\Delta 6S > A$}) and phospho-enabled controls (eS6z^{WT-HA}). Plants were grown at (c) 22°C and (d) 12°C. The cool temperature exacerbates the photosynthesis defect in *rps6b*. The plots are boxplots with the median 25th–75th percentiles of data shown as boxes and the remainder as whiskers.

phospho-enabled eS6^{WT-HA} transgene, as is visually evident from the volcano plots, Venn diagram, and heat map (Figure 5b–d).

The eS6z ^{$\Delta 6S > A$} transgene showed little evidence for gain of function effects, that is, differential gene expression over wild type that cannot be interpreted as a lack of complementation of the *rps6a* and *rps6b* mutations (34 + 4 = 38 genes, i.e., 11% of differentially expressed genes between eS6 ^{$\Delta 6S > A$} versus WT; Figure 5b). This number is barely above the number expected for false discovery, and their fold difference in expression was generally well below two-fold, suggesting they are statistical outliers. If eS6-P played a “moonlighting” role independent of eS6’s role in the ribosome, this role might have revealed itself here in the form of novel aberrations in the gene expression profile, but it did not. Instead, the majority (~90%) of genes that are differentially expressed in eS6z ^{$\Delta 6S > A$} are already

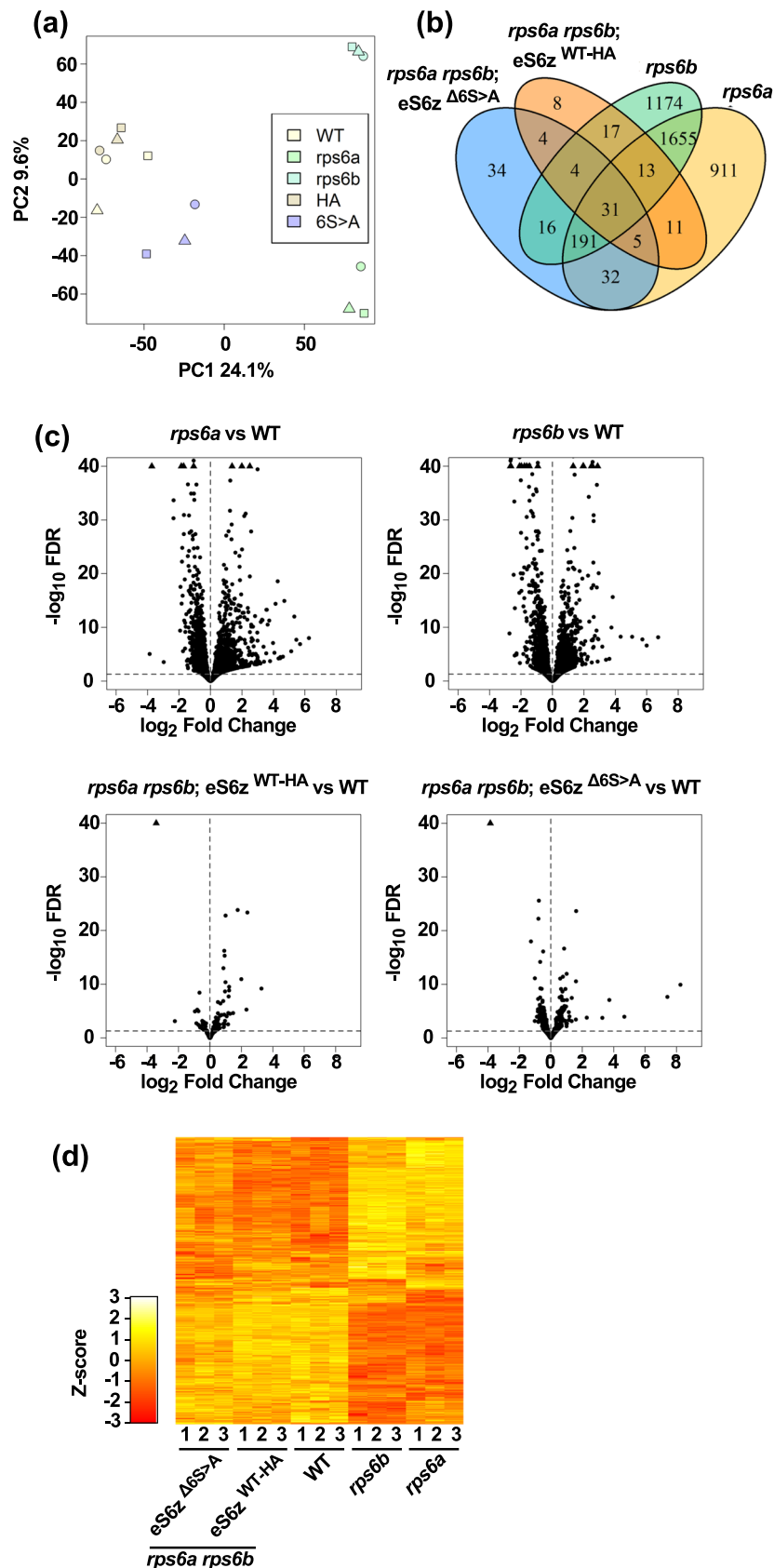
known to be misexpressed in the *rps6* mutants. Most likely these residual weak effects in eS6z ^{$\Delta 6S > A$} are loss-of-function effects; they may be due to the phospho-deficiency or due to a shortfall in eS6 gene expression (see Figure 1c). This is difficult to distinguish rigorously.

The *rps6a* and *rps6b* mutants have a moderate number of paralog-specific gene expression defects (e.g., see Figure 5b,d). Jointly, the two eS6z-based transgenes were about as successful in complementing *rps6b*-specific defects as *rps6a*-specific defects (Figure 5b,d; all but four of the *rps6b*-specific genes and all but five of the *rps6a*-specific genes). This again confirms that the eS6z and eS6y proteins are for the most part functionally equivalent.

For the analysis of the eS6 ^{$\Delta 6S > A$} phospho-deficient strain, we focused on genes and gene ontology terms that distinguish it from the



FIGURE 5 The transcriptome of seedlings with a phospho-deficient eS6z resembles that of wild type but falls short of full functional complementation in specific ways. The transcriptome was characterized by RNA-sequencing from 12-day-old seedlings of five genotypes, wild type, *rps6a* and *rps6b* single mutants, and *rps6a rps6b* double mutants complemented with phospho-enabled (eS6z^{WT-HA}) or phospho-deficient eS6z (eS6z^{Δ6S>A}). (a) Principal component analysis of the 15 samples, three replicates of each genotype. (b) Venn diagram showing the number of differentially expressed genes (FDR < .05, vs. wild type) in various pairwise comparisons. (c) Volcano plots of differential gene expression. The stippled horizontal line marks the false discovery rate (FDR) cutoff of .05 that defines differentially expressed genes. (d) Heatmap of differentially expressed genes. Only genes that passed FDR in at least one of the six relevant pairwise comparisons are included. Genes were filtered with DESeq2, and the display is Z-scored.



eS6^{WT-HA} strain. Of 317 genes that passed FDR, only 13 were altered by more than two-fold (Dataset S1). Gene ontology analysis with TOPGO revealed that many functional categories were misexpressed

in *rps6a* and *rps6b* versus WT (Figure 6), for example, “translation” and “photosynthesis.” Gene-by-gene heatmaps demonstrate that the defects in *rps6a* and *rps6b* were qualitatively if not quantitatively

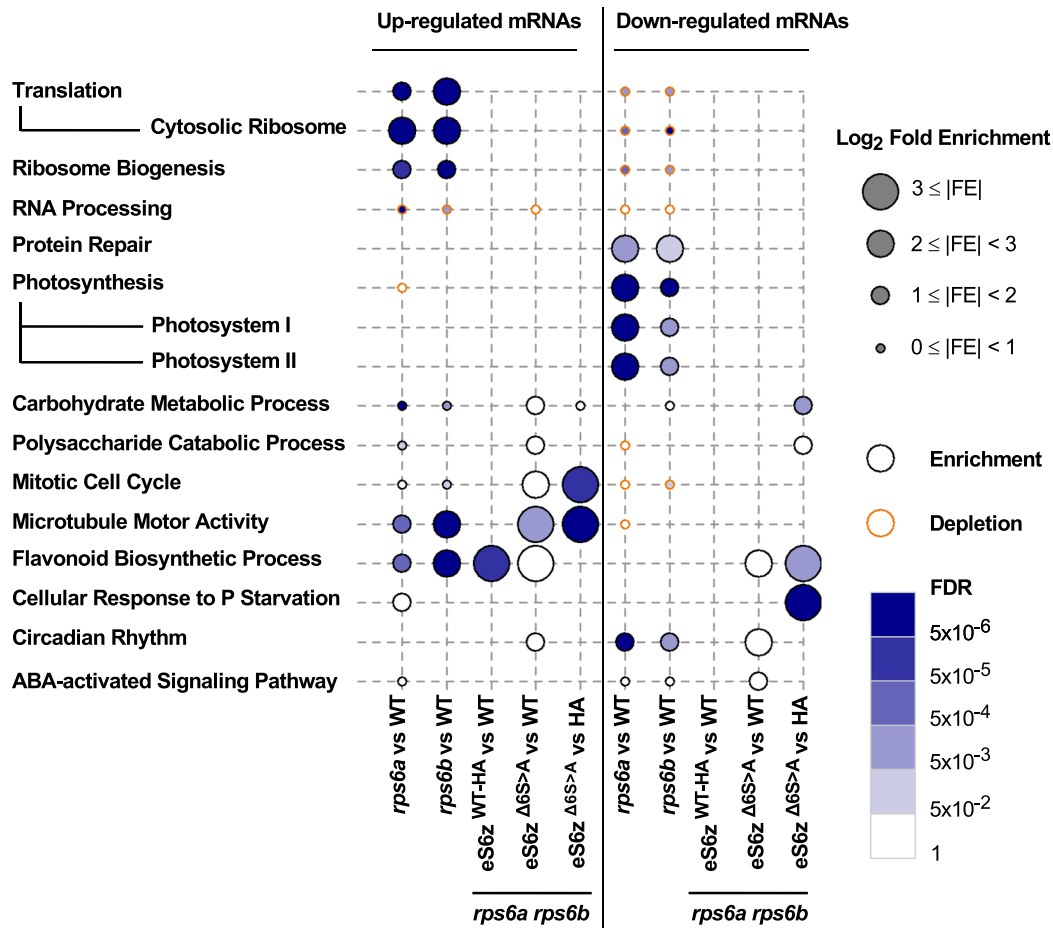


FIGURE 6 RNA-Seq gene ontology (GO) analysis of gene expression defects in eS6 phospho-deficient seedlings and controls. The graphic shows functional trends among genes that were differentially expressed between wild type and *rps6a* or *rps6b* single mutants or wild type and rescued double mutant transgenic lines. The circle size for each GO term indicates the fold-enrichment (FE) of the functional term among the differentially expressed genes over what was expected by chance alone. The fill color indicates the likelihood of false discovery (FDR). The gray perimeter indicates functional enrichment, and the orange perimeter indicates depletion.

the same for most genes (Figure S7A,B,F). Remarkably, these defects were almost fully complemented by both the eS6z^{WT-HA} and eS6z^{Δ6S>A} transgenes. Thus, phosphorylation of eS6z is not required for the expression of most translation-related mRNAs. This result is consistent with our polyribosome analyses (Figures 1d and 2). Likewise, both the eS6z^{WT-HA} and eS6z^{Δ6S>A} transgenes complemented the *rps6* mutants' major deficiencies in "photosynthesis," including the major child terms, photosystem I and II, light harvesting, and photoinhibition (Figure S7B), consistent with the rescue of photosynthetic efficiency, $Q_{y_{max}}$ (Figure 4a–d).

In contrast, several other GO terms were not fully complemented by eS6z^{Δ6S>A}. Prominent among these were "mitotic cell cycle" and "microtubule motor activity" (Figures 6 and S7C–D), which was driven by the upregulation of kinesins. The phospho-deficient eS6 appears to be not fully functional as compared to eS6z^{WT-HA} with respect to microtubule motor or cell cycle functions.

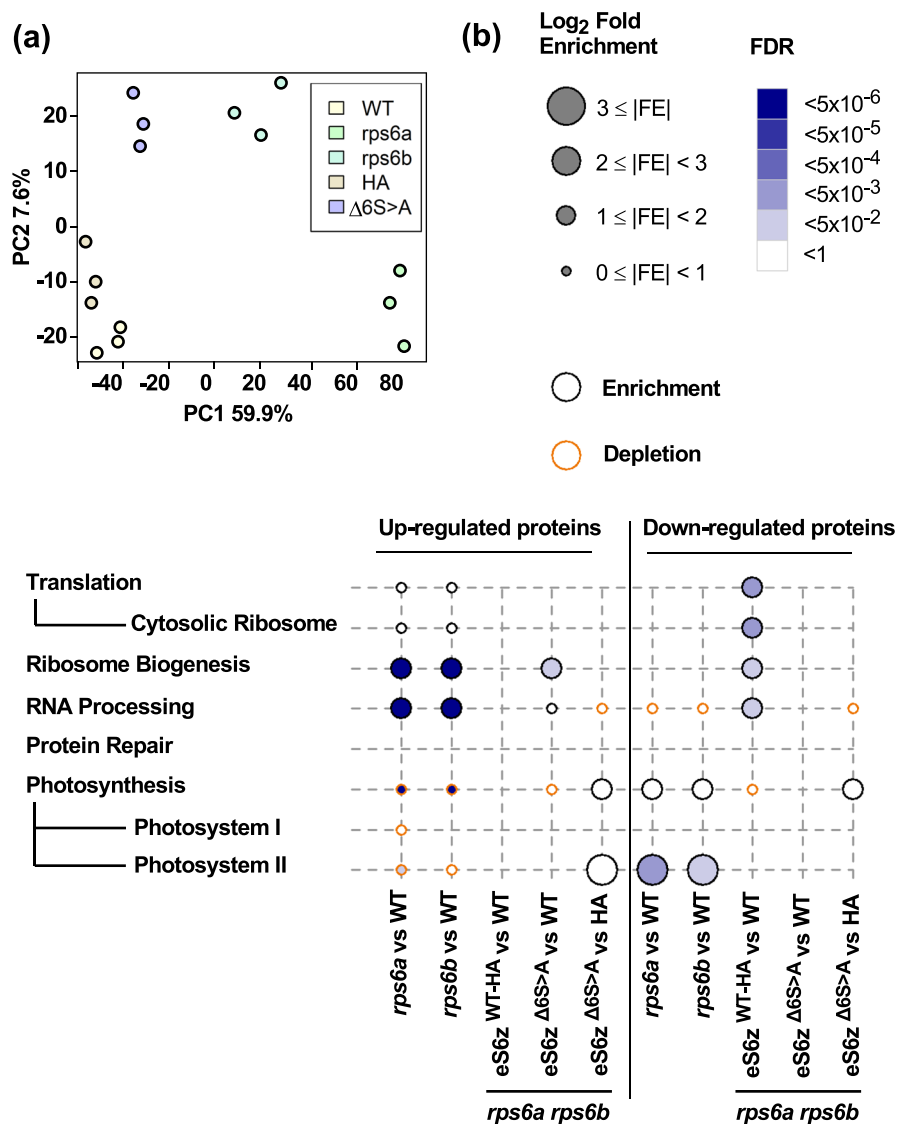
A function specifically altered between eS6z^{Δ6S>A} and eS6z^{WT-HA} was "cellular response to phosphate starvation." These genes were coordinately altered in both *rps6a* and *rps6b*. The eS6z^{WT-HA} slightly

overcomplemented these defects, whereas eS6z^{Δ6S>A} fell slightly short. This caused a notable differential between eS6z^{Δ6S>A} and eS6z^{WT-HA} (Figure 7E). Of 11 genes significantly underexpressed in the phospho-deficient line, four were involved in galactolipid and sulfolipid synthesis (MGD2, MGDC, SQD1, SQD2), besides *PHO* and *PAH* and *SPX* genes involved in other aspects of phosphate homeostasis. This raises the interesting idea that eS6-P may play a role in phosphate homeostasis.

2.6 | Proteome effects in *rps6* single mutants and P-deficient double mutants

To our knowledge, no proteome analysis has been published for Arabidopsis ribosomal protein mutants. We performed mass spectrometry proteomics in triplicate on the same five genotypes previously subject to RNA-Seq. Similar to the RNA-Seq data, the PCA separated the five genotypes based on differential protein abundances (Figure 7a).

FIGURE 7 Proteome of *rps6a* and *rps6b* ribosomal protein single mutants and double mutants complemented with phospho-deficient and phospho-enabled eS6z. Protein samples are from shoots of ~12-day-old seedlings (Figure 6a). (a) Principal component analysis of the triplicate data mirrors the separation of the samples in the RNA-Seq analysis. (b) Differentially expressed proteins that passed a significance threshold were classified by gene ontology. Major enriched terms around ribosomes and photosynthesis are displayed with their enrichment or depletion factor and likelihood of false discovery. For details see Figure 6.



The *rps6a* and *rps6b* mutants were deficient in proteins for photosynthesis, especially photosystem II. They overaccumulated ribosome biogenesis proteins, many ribosomal proteins, and other RNA-related proteins. Although the deficiency in photosynthesis proteins was rescued effectively by both phospho-enabled and phospho-deficient eS6z (Figures 7b and S8A), the excess in ribosomal biogenesis proteins was rescued less well by phospho-deficient eS6z $\Delta 6S > A$ than phospho-enabled eS6z^{WT+HA}. This defect for ribosome biogenesis was more pronounced than that for ribosomal proteins per se and for other RNA-related functions such as RNA degradation and translation initiation (Figures 7b and S8B,C,D). Complementation of photosynthesis and translation defects were both consistent with the RNA-Seq data. These results may suggest that the ability to phosphorylate eS6z represses the mRNA expression or accumulation of proteins for ribosome biogenesis. A role for eS6-P in ribosome biogenesis had previously been suggested in the mouse (Chauvin et al., 2014), although it played out at the transcript level rather than translation.

2.7 | Translation and growth phenotypes in partially phospho-deficient *rps6* single mutants confirm that eS6z phosphorylation is dispensable

In the early work leading up to the fully phospho-deficient plants described earlier, we introduced a series of phospho-mutated eS6z and eS6y transgenes into *rps6a* and *rps6b* single mutants. In the single *rps6* mutants that were complemented with a phospho-deficient allele lacking the six major phosphorylation sites, the second paralog of eS6 remains available to be phosphorylated. We performed immunoblots on whole-cell extracts, as well as on gradient-fractionated material, to address whether eS6y remains phosphorylated when phosphorylation of eS6z is disrupted. In whole-cell extract 2.5 h after lights-on (ZT2.5), three different eS6z^{AS > A} mutants ($\Delta 3S > A$, $\Delta 5S > A$, and $\Delta 6S > A$) had unexpectedly low levels of P-eS6y (Figure 8a). This was not because the antibodies against S237-P and S240-P detected P-eS6y less well, as evident in the single-mutant *rps6a* lane (also see Figure 2e). In eS6z^{AS > D} mutants, phosphorylation was reduced only

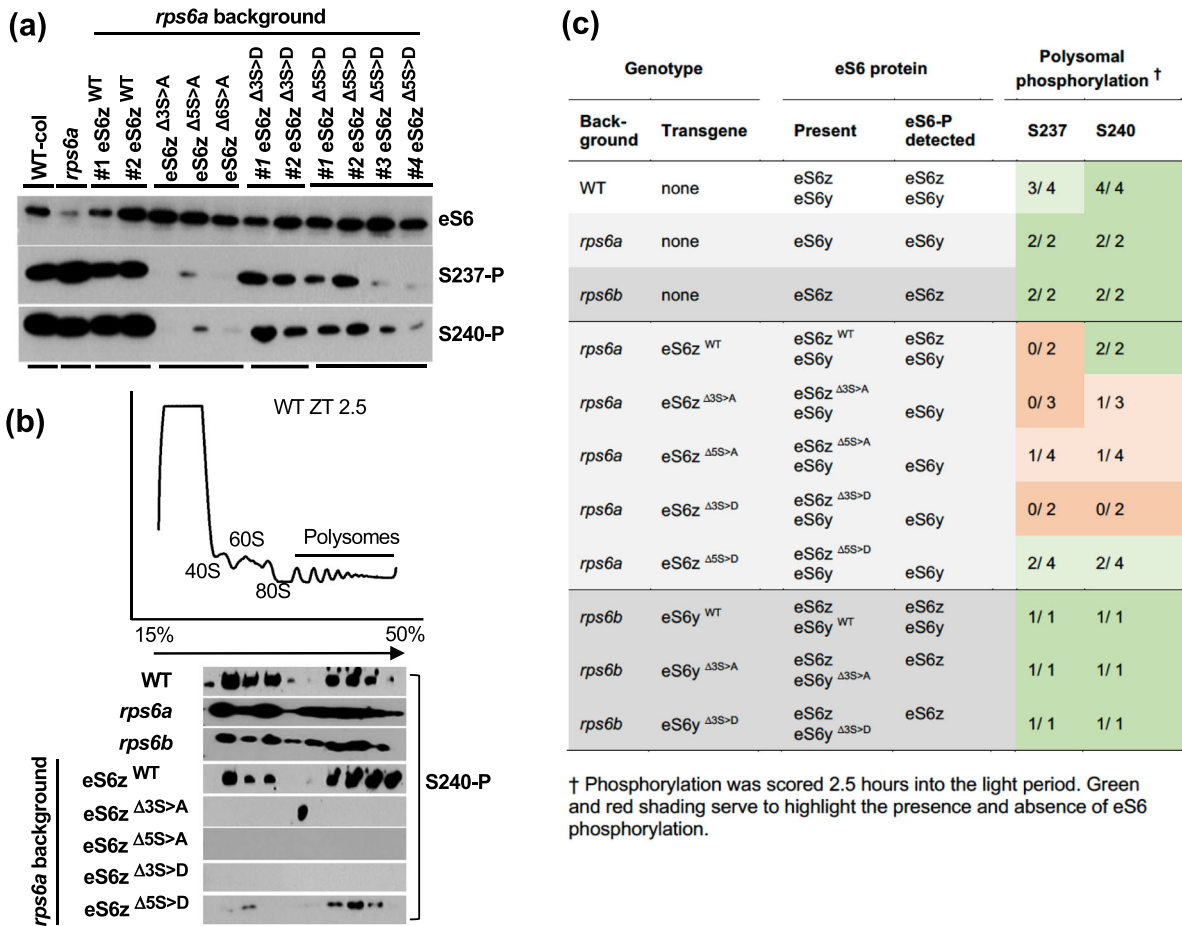


FIGURE 8 Phosphorylation status of eS6 in *rps6* single mutants that were complemented with wild-type or phospho-deficient alleles of eS6. Both S > A and S > D mutations are shown. (a) Whole-cell extracts from seedlings in the *rps6a* background were probed for phosphorylation of S237 and S240 on western blots using phospho-specific antibodies and for total eS6 with an eS6 antibody. Several lines were analyzed in duplicate. (b) Polysome gradients from seedlings harvested 2.5 h after lights-on (ZT2.5). The absorption profile at the top comes from *rps6a* harboring eS6z^{Δ6S>A} and is shown as a representative. The other gradients looked similar. Shown below are immunoblots of *rps6a* single mutants complemented with various phospho-deficient alleles; gradient fractions 3–12 were probed for phosphorylated S240 (S240-P). *rps6a* and *rps6b* and wild type serve as positive controls. (c) Phosphorylation of eS6 in polysomes. Summary of data from western blots such as those in panel (b). The fractional data (e.g., 1/4) indicate the proportion of replicate experiments in which phosphorylation of eS6 was detected. In the remaining replicates, phosphorylation was undetectable or weak.

mildly and less consistently. eS6y phosphorylation was also reduced in polysome gradients from these S > A mutant lines (Figure 8b), with data from many additional blots summarized in Figure 8c. Although we also examined phosphorylation of eS6z protein when *rps6b* mutants were complemented with phospho-deficient eS6y, the results were not as extensive and did not show the loss of phosphorylation in eS6z (Figure 8c).

Taken together, these data suggest that the phospho-deficiency in eS6z^{ΔS>A} interferes with the phosphorylation of the eS6y paralog. Although we do not know the mechanism, this unexpected observation of poor eS6-P is important, because it implies that the *rps6a* plants that were complemented with phospho-deficient eS6z were substantially free of eS6-P, at least at the sites S237 and S240 that could be assessed by specific antibodies. The suppression of phosphorylation on the eS6y paralog is our only clear effect of the phospho-deficiency in eS6 on the translation apparatus.

Although the single *rps6a* eS6z^{ΔS>A} mutants had low eS6 phosphorylation, the slow root growth in *rps6a* was complemented well by several phospho-deficient isoforms of eS6z, just as well as by phospho-mimic and HA-tagged wild type eS6z (Figure 9a–d). The *rps6b* mutation was also complemented, but root growth was slower than wild type with three eS6y^{ΔS>A} alleles tested (Figure 1e–f). The incomplete complementation by eS6y isoforms cannot be attributed to the phospho-deficiency of eS6y because the wild-type *RPS6B* genes also did not fully complement the *rps6b* mutation, as shown earlier (Creff et al., 2010; Figure S3C). These results extend the work in the double mutant background and suggest that it is not necessary for each paralog of eS6 to be phosphorylatable. Phosphorylation appears to be a physiologically dispensable property of eS6 under our growth conditions.

We then examined by sucrose density gradients whether overall polysome loading was altered in the phospho-deficient single mutants.

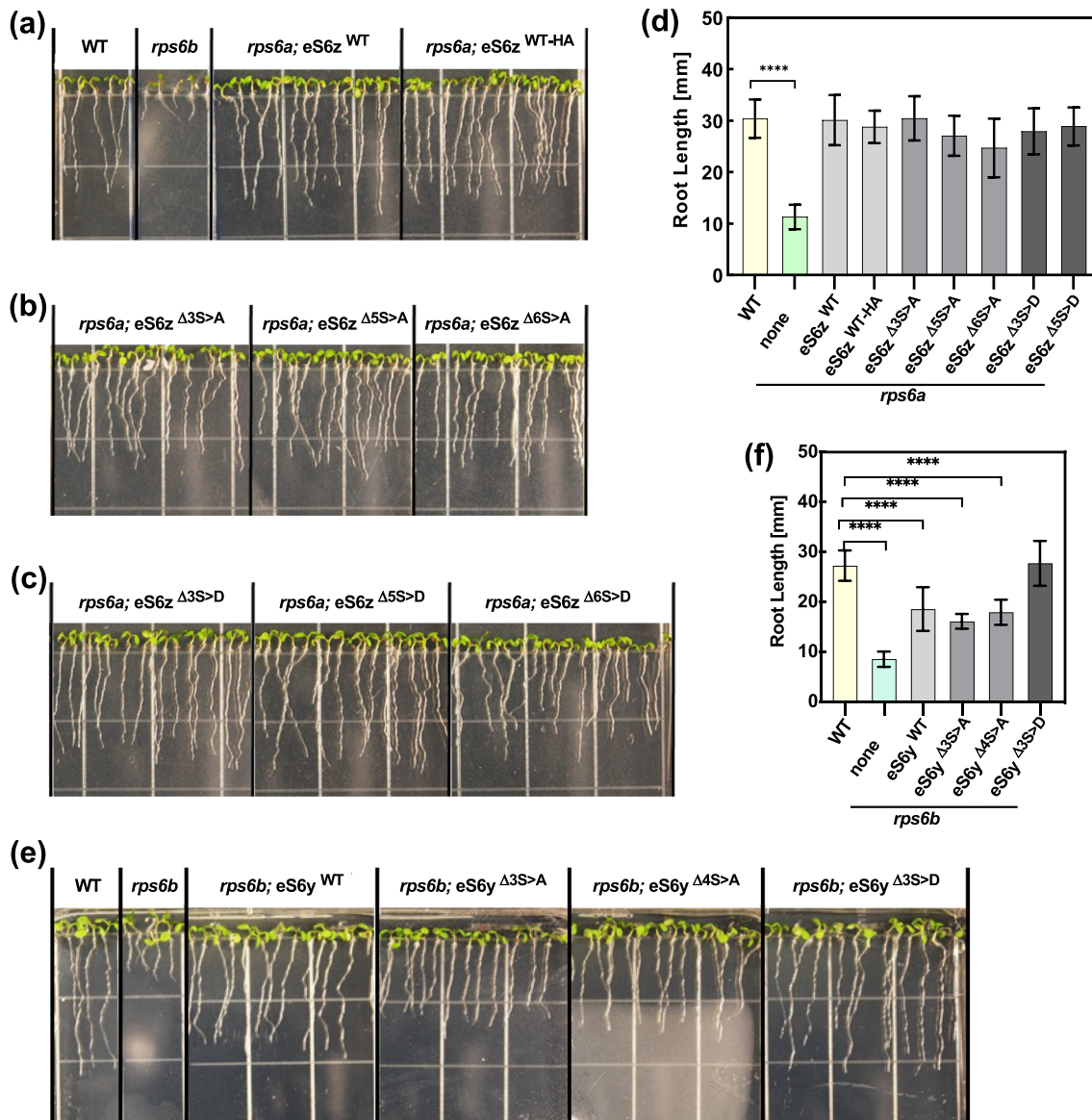


FIGURE 9 Phospho-deficient alleles of eS6z and eS6y substantially complement *rps6* single mutant root growth defects. (a) Wild-type, (b) phospho-deficient, and (c) phospho-mimic alleles of eS6z complement the root growth defect of the *rps6a* mutation. (d) Quantitation of root lengths from lines in (a–c). (e, f) Phospho-deficient and phospho-mimic alleles of eS6y partially complement the *rps6b* mutation.

Quite clearly, in the phospho-deficient single mutants (*rps6a*; *RSP6B*; eS6z^{Δ3S>A} or ^{Δ5S>A}), the dark-to-light transition triggered the typical rise in polysome loading (Figure S9), just as in wild type and in the *rps6* mutants. Therefore, the phospho-deficient single-mutant plants had no striking defects in polysome loading. The significant elevation in the level of the 60S subunit seen earlier in the single *rps6a* mutants was no longer significant with the phospho-deficient eS6z transgenes. Similar results were also obtained when the *rps6a* mutation was complemented with phospho-mimic versions of eS6z (Figure S9). These results suggest that the phospho-deficient isoform rescues the ribosome biogenesis defects. Because each ribosome contains only one molecule of eS6, and because we know of no mechanism that would prevent eS6z and eS6y-containing ribosomes to mingle on the same mRNA molecule, it appears that polyribosomes with a mixture of

phosphorylatable and unphosphorylatable ribosomes can function adequately in global translation.

3 | DISCUSSION

3.1 | New phenotypes of ribosomal protein mutants

Despite decades of research on the role of ribosomal protein S6 phosphorylation, its biological effect remains unclear in plants. Our analysis discovered several new phenotypes of *rps6* mutants. The two cotyledons of *rps6* mutants often differ in size. The pale green color of the seedlings and rosette-stage plants is accompanied by defects in gene

expression of many photosynthetic genes and by reduced quantum efficiency of photosystem II, an effect exacerbated at cooler temperature. The *rps6a* and *rps6b* mutants have an excess of free 60S subunits, which was reported previously in yeast and Arabidopsis (Creff et al., 2010; Pachler et al., 2004) but is documented here with additional statistical support. We also provide one of the first transcriptome datasets from mutants in plant cytosolic ribosomal proteins and, to our knowledge, the first that compares mutations in multiple paralogs. The *rps6a* and *rps6b* mutant transcriptomes are largely similar but differ in a few areas. In *rps6a*, the photosynthesis functions are more strongly affected than in *rps6b*, whereas in *rps6b*, the cytosolic translation functions are more strongly upregulated than in *rps6a*. The plastid ribosomes do not feature prominently. Because transgenes of eS6z that use the *RPS6A* promoter complemented the defects well, we suspect that the difference in phenotype is not due to differences in the amino acid sequences of eS6z and eS6y. Instead, this difference could arise if eS6y had a shifted spatial expression pattern, biased toward growing cells, which produce more ribosomes, rather than cells fated to become mesophyll, which produce the photosynthetic apparatus.

We also present the first proteomics data for plant ribosomal protein mutants. Defects include a drop in photosynthesis functions and an upregulation of ribosomal proteins and ribosome biogenesis proteins in both *rps6a* and *rps6b*, consistent with the transcriptome data. The *rps6a* mutant has strongly elevated levels of a subset of ribosomal proteins and even more strongly for ribosome biogenesis proteins. This same effect is also seen in *rps6b*, mostly for the same ribosomal proteins. In each mutant, the other paralog is upregulated, together with many other ribosomal proteins. Together, these results suggest the mutants' growth is rate limited by the production of *RPS6* mRNA. In the *rps6b* mutant, it takes arguably twice as long to accumulate enough *RPS6* mRNA per cell than in wild type. Hence, the mutants grow more slowly. Meanwhile, they accumulate excess mRNAs for other ribosomal proteins, whose gene dosage is normal, and which overaccumulate as a result. Ribosome biogenesis proteins are expressed at a higher level as well, perhaps driven by the excess of yet-to-be-assembled ribosomal proteins.

3.2 | eS6z and eS6y paralogs are functionally equivalent

We looked for evidence that the z and y paralogs of eS6 have different functions. In short, our data suggest that the two paralogs are functionally equivalent. First, the eS6y paralog was able to complement the *rps6a* mutant phenotype as well as the eS6z paralog, with respect to root growth and general appearance, as observed earlier (Creff et al., 2010; Ren et al., 2012). Second, the double mutant *rps6a rps6b* was complemented effectively by eS6z^{WT-HA}, a hemagglutinin-tagged version of eS6z, as well as a wild-type version of eS6y. Even though both wild-type alleles were absent, both eS6z and eS6y were able to complement essentially completely and equally. The phenotypic rescue was evident at the biochemical level (polysome profiles

and loading), photosynthetic efficiency, root growth, and other developmental phenotypes. We note here that the single mutant *rps6b* was complemented incompletely by either eS6z or eS6y, a result that we hypothesize may be due to residual mRNAs from the *RPS6B* gene interfering with transgene expression. In keeping with this explanation, in the *rps6a rps6b* double mutants, complementation with wild-type *RPS6* genes was complete, and coincidentally, the RNA-Seq data showed that the residual transcripts from the mutated *rps6b* gene were suppressed.

3.3 | Phospho-deficient eS6 performs many functions of the wild-type eS6

Light, sucrose, and auxin can boost translation. These signals also boost TOR activity, which then causes phosphorylation of eS6 in its C-terminus. This has led to the hypothesis that eS6-P is causally involved in mediating effects on translation. However, evidence for this idea has been mostly correlative (Boex-Fontvieille et al., 2013; Chen et al., 2018; Dobrenel et al., 2016). For example, eS6-P is accompanied by increased expression of plastid ribosomal proteins (Dobrenel et al., 2016) and by increased polysome loading in the cytosol (Chen et al., 2018; Liu et al., 2012); however, our data indicate that eS6-P-deficient plants express chloroplast ribosomal proteins normally and can increase polysome loading in the morning as effectively as wild type. Recently, Mancera-Martinez et al. addressed this question by manipulating the phosphorylation potential of eS6 by expressing $\Delta S > A$ and $\Delta S > D$ versions of eS6y from a cauliflower mosaic virus 35S promoter in *rps6a* single-mutant plants. Similar to our data, the two versions did not differ in global polysome loading. However, the two versions differed in the translation of two reinitiation-dependent reporter mRNAs, suggesting that eS6 phosphorylation may regulate the translation of specific mRNAs (Mancera-Martinez et al., 2021).

Here, we sought out evidence to reveal the role of eS6 phosphorylation by comparing the biochemical, molecular, cellular, and organ-level phenotypes of *rps6* double mutants complemented with either a phosphorylation-enabled allele (WT-HA) or a phosphorylation-deficient allele ($\Delta S > A$). This is the first plant study to examine P-deficient alleles in a genetic background mutated for both *RPS6* paralogs. It is also the first to compare the plant P-deficient eS6 against the wild type, rather than P-deficient against P-mimic (Mancera-Martinez et al., 2021). We chose the eS6z paralog, rather than both eS6z and eS6y for simplicity. This was a reasonable choice because eS6z and eS6y were confirmed to be functionally equivalent. We constructed the phospho-deficient allele as close to the native version as possible. Aside from keeping its native promoter, untranslated regions, and exon-intron structure, we left it untagged in order to not introduce confounding features. We did tag the corresponding wild-type eS6z with HA to be able to distinguish it from the native version, but our data suggest that this did not compromise its function. We created a series of phospho-deficient versions of eS6z and eS6y anticipating that this would allow us to define the minimal



changes necessary for a robust phenotype. In the end, a version with six codons altered to alanine revealed only rather subtle phenotypes, and therefore, we did not pursue the versions with fewer changes in detail. However, data from other $S > A$ and $S > D$ alleles are included in this article because their results reinforce those for the main $\Delta 6S > A$ allele.

Overall, the phospho-deficient eS6z proved to be functional. It reverted the lethal phenotypes of the *rps6a rps6b* double mutant; polysome loading was normal, including the increase in polysome loading during the daily dark-to-light transition. And although *rps6* single mutants had an excess of the 60S ribosomal subunit, the phospho-deficient double mutants reverted back to normal levels. The phospho-deficient eS6z also partitioned to cellular compartments, nucleus, nucleolus, and cytosol, similarly to wild type. The phospho-deficient eS6 rescued the gene expression defects commonly seen in *rps6a* and *rps6b* mutants, as well as the misregulation of protein levels in translation and photosynthesis. Accordingly, photosynthetic efficiency was near normal levels.

We want to emphasize that our conclusion is not solely based on the *rps6a rps6b* double mutants. Even in *rps6a* single mutants, surprisingly, the presence of a phospho-deficient eS6z suppressed the phosphorylation of the eS6y paralog, yet rescued the polysome profiles of *rps6a* and allowed for normal growth. Although we can only speculate about the mechanism for this coordinated loss of phosphorylation, this result bolsters the conclusion that phospho-deficient eS6 is largely functional, and ribosomes lacking eS6 phosphorylation are functional as well.

3.4 | Emerging roles of eS6 phosphorylation

Detailed analysis of the phospho-deficient plants did, however, reveal several notable abnormalities and deficiencies. The YFP-tagged eS6z $\Delta 7S > A$ tended to aggregate a bit more readily in the nucleus than did the wild-type version. In the gene expression profile, certain defects in the mitotic cell cycle functions and responses to phosphate starvation, which are characteristic of *rps6* mutants, failed to get fully rescued by the phospho-deficient $\Delta 6S > A$ allele, although they were rescued by the phospho-enabled WT-HA allele. A transient pointed-leaf phenotype suggested that leaf expansion was slightly delayed, as was the rate of root elongation, a sensitive indicator of cell division. At the proteome level, certain misregulations of ribosome biogenesis proteins also failed to get fully rescued. In this context, it is notable that eS6 functions as part of the small subunit processome in yeast ribosome biogenesis (Bernstein et al., 2004). The increase in ribosomal proteins and the excess free 60S subunit seen in our *rps6* mutants mirrors similar increases in yeast and mammalian ribosomal protein mutants (Pachler et al., 2004; Robledo et al., 2008).

Together, these results are our best indicator as to the cellular function of eS6-phosphorylation in Arabidopsis. The phospho-deficient plants had morphological defects as seedlings, cotyledon asymmetry, and pointed leaves. Although these phenotypes were more transient than in the original *rps6* mutants, meaning they had

largely disappeared at the time when RNA was harvested for transcriptome profiling, it is plausible that it was the misregulation of cell cycle-related mRNAs and ribosome biogenesis proteins that led to the growth inhibition in cotyledons and first leaves.

It was plausible that the eS6 phospho-deficient plants might reveal a phenotype not seen in *rps6* mutants, a gain-of-function defect. However, few if any of the defects observed in the phospho-deficient plants look like a clear gain-of-function defect. Instead, the phenotypes in the *rps6a rps6b* eS6z $\Delta 6S > A$ line are incomplete rescues of defects germane to *rps6a* mutants. A few individual genes show the gain-of-function pattern, that is, abnormal expression in $\Delta 6S > A$, but normal expression in all other genotypes. Very few genes match this pattern, including ADC2 and RD19, CR88 and CYP707A2, CHIL and RHM1, and BBD1. These genes may be the rare sentinels of eS6-phosphorylation, but this inference is not strong, because these genes may also be false negatives for differential expression in the *rps6a* and *rps6b* mutants, and they are not legitimized by belonging to a functionally defined gene ontology group.

This study has a number of limitations. Although the phospho-deficient version of eS6z was expressed at a level higher than the native eS6z, it did not quite reach the two-fold increase one would have preferred. Our proteome data in the *rps6a rps6b* background pegged eS6z $\Delta 6S > A$ at 1.6-fold the level of eS6z in wild type. Because *RPS6A* and *RPS6B* are expressed equally, the total level of transgenic eS6 protein was 20% below wild type. We consider this acceptable because *rps6a* heterozygotes, whose gene dosage is 25% below wild type, do not have major phenotypes, that is, *rps6a* and *rps6b* are recessive mutations, as is also true for other *rps* mutations (Van Lijsebettens et al., 1994). Our work also did not check for phenotypes under stress conditions, with photosynthesis at 12°C as one exception. It is possible that the P-deficient plants might reveal additional growth defects under conditions that alter eS6-P, such as hypoxia, heat, or high light and extended darkness.

Taken together, our data together with those of Mancera-Martinez and coworkers (Mancera-Martinez et al., 2021) extend what we know about the functional consequences of eS6-P to plants. In each eukaryote that has been studied, yeast, mammals, and now plants, global translation is largely unaltered (Ruvinsky et al., 2005; Yerlikaya et al., 2016), although Wittenberg and coworkers reported a lower rate of translation and increased translation fidelity in eS6-P-enabled mouse cells (Wittenberg et al., 2016). Evidence for effects on mRNA-specific translation exists but is sparse (Bohlen et al., 2021; Mancera-Martinez et al., 2021; Puighermanal et al., 2017). This is also true for effects at the transcriptome and proteome level (Yerlikaya et al., 2016, and this work). These minimal phenotypes stand in contrast to the diverse consequences of the environmental stimuli that regulate eS6-P and the diverse phenotypic effects from inhibiting the TOR-S6 kinase pathway genetically or pharmacologically (Ahmad et al., 2019; Ingargiola et al., 2023; Margalha et al., 2019; Ren et al., 2012; Scarpin et al., 2022). Yerlikaya and coworkers (Yerlikaya et al., 2016) concluded conservatively that none of their phenotypes in eS6 P-deficient yeast could be firmly ascribed to the P-deficiency but were probably due to reduced eS6 protein levels. For this work in

Arabidopsis, we like to propose a similar caveat. Essentially, all the phenotypes seen in eS6 phospho-deficient plants are also seen in *rps6* mutants. They are hypomorph (loss-of-function) phenotypes rather than neomorph (gain-of-function) phenotypes. It is therefore difficult to rule out that these phenotypes are due to the reduced level of the eS6^{Δ6S>A} protein or subtle insufficiencies in its pattern of expression, rather than its lack of phosphorylation.

4 | MATERIALS AND METHODS

4.1 | Arabidopsis strains and genotyping

For *RPS6A* (At4g31700), the *rps6a-2* allele is line GK_468C04 from the GABI-KAT T-DNA collection with an insertion in intron 4 (Kleinboelting et al., 2012). For *RPS6B* (At5g10360), the *rps6b-1* allele is SALK_012147C from the SALK collection with an insertion in exon 4 (Creff et al., 2010).

rps6a-2 and *rps6b-1* seedlings were genotyped via PCR to check for the presence of the WT *RPS6* gene and the T-DNA insertion. LP and RP primers that span the T-DNA insertion site were used to amplify the WT fragment, which is ~1 kb in size. LP and T-DNA LB (GabiKat) primers were used to amplify the T-DNA region, which is ~7 kb. Similarly, for *rps6b-1* seedlings, LP and RP primers were used to amplify the WT fragment and RP and TDNA LBb 1.3 (SALK) primers were used to amplify the T-DNA fragment. Annealing temperatures of 56 and 54.3°C were used for *rps6a-2* and *rps6b-1* reactions, respectively.

To analyze the segregation of the transgenes, seedlings were grown on 1/2 strength MS medium supplemented with 1% sucrose with either 50 µg/ml kanamycin, 7-µg/ml sulfadiazine, or Basta. Fifty seeds were plated on either kanamycin or sulfadiazine to score the 3:1 segregation of *rps6b-1* or *rps6a-2*, respectively, and 70 seeds were plated on Basta plates to score for a 3:1 or 15:1 or 63:1 segregation of the transgene. Resistance versus sensitivity was scored 7 days after plating, and a Chi-square test was performed to confirm the segregation ratio. The line was then planted in soil, and the progeny from the plants was again scored the same way on the way to identify families homozygous for *rps6a-2*, *rps6b-1*, and a transgene.

4.2 | RNA and protein methods

For reverse-transcription PCR, WT, *rps6a-2*, and *rps6b-1* seedlings were grown on 1/2 strength MS salt medium for 12 days and the tissue was harvested for RNA extraction using the Zymo Research ZR Plant RNA Mini Prep Kit. cDNA was synthesized from the total RNA, and the *RPS6A* and *RPS6B* transcripts were amplified via PCR using PrimeStar Max polymerase (Takara). The PCR products were separated on a 1% agarose gel. SDS-PAGE and immunoblotting with phosphospecific antibodies were performed as described (Enganti et al., 2018).

4.3 | Polysome profiling

The aerial portion of 12 days-after-germination seedlings grown under long-day conditions was collected by flash freezing at ZT23.5 (30 min before lights on) and ZT2.5 (two and a half hours after lights on). Plant tissue was ground in liquid nitrogen and extracted in polysome isolation buffer (200 mM Tris-HCl pH 8.4, 25 mM MgCl₂, 50 mM KCl, 1% deoxycholic acid, and 2% polyoxyethylene 10 tridecyl ether). Sucrose gradients were prepared by layering 1.7, 3.3, 3.3, and 1.7 ml each of 50% sucrose, 38.4% sucrose, 26.6% sucrose, and 15% sucrose, respectively. After the addition of each gradient layer, the centrifuge tube was frozen at -80°C for 1 h. On the day before use, the gradients were thawed overnight without shaking at 4°C. Plant extracts (1 ml) were loaded on top of a 10 ml 15%–50% sucrose gradient and centrifuged at 35,000 rpm for 3.5 h without brake (Beckman Coulter SW 41Ti). After recording the RNA absorbance profile at 254 nm, the gradient was fractionated into 12 equal fractions. Samples from the fractions were then separated on SDS-PAGE gels followed by immunoblotting to determine eS6 protein levels and phosphorylation levels in the samples. Equal volumes of sample from each fraction were loaded onto the gels.

The areas under the curve for the polysome profile traces were calculated as described (Enganti et al., 2018; Lokdarshi, Guan, et al., 2020). In brief, gradient traces were manually split into 40S, 60S, 80S, small polysomal (2–4 ribosomes), and large polysomal sections (5+ ribosomes). Blank gradient traces were subtracted from the sample traces, and the area under the curve was calculated for each section. If applicable, areas were combined into non-polysomal (sum of areas from 40S, 60S, and 80S) and polysomal (sum of areas from small and large polysomal) sections. Abundances of different ribosomal complexes were compared between genotypes or time points by using Welch's t-test.

4.4 | Transient gene expression in *Nicotiana benthamiana*

Coding sequences of eS6 were cloned as N-terminal fusions to enhanced yellow fluorescent protein and expressed from the CaMV 35S promoter. Overnight cultures of *Agrobacterium tumefaciens* harboring the T-DNA plasmid of interest were grown with appropriate antibiotics. The cultures were pelleted and resuspended in infiltration buffer (10 mM MES buffer, 10 mM MgCl₂, pH 5.4) to an optical density of 1.0 at 600 nm. Acetosyringone was added to a final concentration of 200 µM to the culture and incubated with agitation for 2 h. Young leaves on 3-week-old *N. benthamiana* plants were infiltrated with the cultures using a 1-ml syringe. The plants were kept in the dark overnight and shifted to normal growth conditions for 36 h following which the leaves were imaged to detect fluorescence by confocal laser scanning microscopy.



4.5 | Root phenotyping

To measure root lengths, seedlings were grown vertically on square petri plates with a grid and photographed on day 7 after germination. Images were imported into ImageJ, and root lengths were measured by tracing each primary root using the segmented line tool.

4.6 | Photosynthetic efficiency measurement

The maximum quantum yield of photosystem II (PS II) ($Q_{Y_{max}} = F_v/F_m$) was measured on a FluorCam 800MF (Photon Systems Instruments, Drásov, Czechia) as per the manufacturer's instructions and modifications (Murchie & Lawson, 2013). Briefly, plants were dark adapted for 1 min (F_0) prior to applying a saturating pulse of $1800 \mu\text{Ein m}^{-2} \text{s}^{-1}$ for .8 s (F_m). Variable fluorescence (F_v) was calculated as the difference between F_0 and F_m to get the maximum quantum yield (F_v/F_m) (Lokdarshi, Morgan, et al., 2020).

4.7 | Molecular cloning and site-directed mutagenesis

RPS6A and RPS6B were amplified from WT Col-0 genomic DNA using primers with added restriction sites: *EcoRI* and *XbaI* for *RPS6A* and *SbfI* and *PvuI* for *RPS6B*. The amplified product was approximately 3 kb, which included the full-length transcribed region, 1.5 kb upstream of the 5' UTR, and 200 bases downstream of the 3' UTR. Both *RPS6A* and *RPS6B* fragments were digested and then ligated to the T-DNA vector pFGC19 (Kim et al., 2007) that was previously digested with the appropriate enzymes. Site-directed mutagenesis was done by PCR with mutagenic oligonucleotide primers in pFGC19. Serine and threonine codons were mutated sequentially to either alanine (GCT) or aspartate (GAT).

Initially, two fragments were generated by PCR with a single codon substitution in the forward and the reverse strand. The primers that were used generated PCR 1 and PCR 2 fragments of 800 and 500 bp for *RPS6A* and 1200 and 500 bp for *RPS6B*, respectively. The products from PCR 1 and 2 were subsequently mixed to serve as template for PCR 3 to generate a longer fragment with the desired mutation that could then be ligated to pFGC19 harboring the respective RPS6 gene. The PCR 3 products were 1.3 kb for *RPS6A* and 1.7 kb for *RPS6B*. The PCR 3 products were purified using a DNA cleanup kit and then digested with either *BstBI* or *XbaI* for *RPS6A* or *XhoI* and *PvuI* for *RPS6B*. *BstBI* and *XhoI* are internal sites within the coding region of *RPS6A* (between intron 3 and 4) and *RPS6B* (exon 2), respectively. *RPS6A* fragments were digested for 30 min at 65 C (*BstBI*) followed by 30 min at 37 C (*XbaI*), whereas *RPS6B* fragments were digested at 37 C for 1 h. The digested products were then run on a gel and purified using a gel extraction kit. The digested fragments were then ligated to pFGC19 digested with the appropriate enzymes in a 3:1 and 1:1 molar ratio of the insert to the vector along with a control that had the cut vector and no insert. The ligation was carried out for 2 h at 16 C. The ligation products were then transformed into competent Top10 cells

via heat shock. The culture was plated on LB plates containing kanamycin and incubated overnight. Colonies were then grown for plasmid extraction and the mutations were confirmed by DNA sequencing. Wild-type and mutant T-DNAs were transformed into *rps6a-2 rps6b-1* double heterozygote plants that had been generated by genetic crossing and transgenic seedlings selected for Basta resistance.

4.8 | RNA-Seq library construction and sequencing

RNA-seq was performed on WT, *rps6a-2*, *rps6b-1*, *rps6a-2 rps6b-1*; eS6z^{WT-HA}, and *rps6a rps6b*; eS6z^{Δ65 > A} genotypes grown under long day conditions. Twelve days after germination, the aerial portions of the seedlings were harvested by flash freezing in liquid nitrogen in the morning. Total RNA was extracted using a commercial kit. RNA quality was measured using a Bioanalyzer (Agilent). Paired-end cDNA libraries were constructed using the Illumina Stranded Total RNA Prep with Ribo-Zero Plus. The libraries were sequenced on a NextSeq in paired-end mode and with 75 base pair long reads at the Oklahoma Medical Research Foundation (Oklahoma City, USA). Raw read quality was assessed with FastQC v0.11.5. Raw reads were aligned to the TAIR10.1 genome and Araport11 annotation using STAR-2.7.7a (Dobin et al., 2013), with default parameters except for the following: -alignIntronMax 1000. Mapping quality was assessed with RSeQC v4.0.0 (Wang et al., 2012). Reads were counted using subread featureCounts v2.0.1 (Liao et al., 2014) in paired-end mode.

4.9 | RNA-Seq differential gene expression

Differential gene expression was performed in R (v3.6.3). Genes that were not expressed in all three replicates of at least one sample were removed. Samples were inspected for batch effect by principal component analysis, and no batch effect was found. The filtered reads were then normalized, and pairwise comparisons between genotypes were performed using DESeq2 v1.26.0 (Love et al., 2014). The resulting *p*-values were corrected for multiple comparisons using FDR with Benjamini–Hochberg parameters and the resulting log₂ fold changes were shrunk using ash2.2 (Stephens, 2017).

Gene ontology analysis was performed on each pairwise comparison using a custom wrapper around the topGO package version 2.38.1 (Alexa & Rahnenführer, 2016). Only genes measured as expressed were used as the gene universe. topGO was run with node size 1 and FDR *p*-value adjustment using a custom script and the classic Fisher, parent-child, and weight01 algorithms. Packages were obtained from CRAN or Bioconductor version 3.7 (Huber et al., 2015).

4.10 | Proteomics

Protein digestion was performed as previously described (Enganti et al., 2018). In brief, samples of 12-day-old light-grown seedlings were suspended in a detergent lysis buffer (2% sodium dodecyl sulfate and 10-mM dithiothreitol in 100-mM ammonium bicarbonate)

supplemented with Halt Phosphatase Inhibitor Cocktail (Thermo Fischer Scientific) for crude protein extraction. Cell debris was removed, and proteins were alkylated with iodoacetamide (30 mM) and incubated in the dark at room temperature for 15 min. Proteins were precipitated via methanol/chloroform/water precipitation and protein pellets were washed twice with methanol. Dried protein pellets were resuspended in 1 ml of 8 M urea and incubated at room temperature for 1 h. Samples were digested via the addition of two aliquots of sequencing-grade trypsin (Promega, 1:50 [w:w]) at two different sample dilutions, 4 M urea (overnight) and subsequent 2 M urea (5 h). Following digestion, samples were adjusted to 1% formic acid and desalted using solid-phase C18 extraction cartridges (Sep-Pak Plus Short, Waters) and lyophilized. All samples were analyzed on a Q Exactive Plus mass spectrometer (Thermo Scientific) coupled with an Easy-nLC 1200 (Thermo Fischer Scientific). For each sample, a single 1- μ g injection of peptides was separated on an in-house-pulled nanospray emitter of 75- μ m inner diameter containing 25 cm of Kinetix C18 resin (1.7 μ m, 100 Å, Phenomenex) across a linear organic gradient of 0%–22% (80% acetonitrile, .1% formic acid) over 210 min at 200 nl/min. Mass spectra data were acquired with the Thermo Xcalibur software using the top 10 data-dependent acquisition. All MS/MS spectra collected were processed in Proteome Discoverer version 2.2 with MS Amanda (Dorfer et al., 2014) and Percolator (Käll et al., 2007). The spectra were searched against the UniProt reference proteome (Proteome ID UP000006548) to which common laboratory contaminants were appended. The following parameters were used by MS Amanda to derive fully tryptic peptides: MS1 tolerance = 5 ppm; MS2 tolerance = .02 Da; missed cleavages = 2; Carbamidomethyl (C, + 57.021 Da) as static modification; and oxidation (M, + 15.995 Da) and carbamylation (N-terminus, + 43.006 Da) as dynamic modifications. The Percolator FDR threshold was set to 1% at the peptide-spectrum match and peptide levels. Protein abundances were calculated by summing peptide abundances determined by the “feature mapper” and “precursor ions quantifier” nodes in Proteome Discoverer 2.2. Using InfernoRDN software (<https://github.com/PNNL-Comp-Mass-Spec/InfernoRDN/releases>), relative protein abundances were first normalized by LOESS across biological replicates and then normalized by a mean central tendency adjustment across the experimental dataset. Pairwise *t*-tests were performed between protein abundances using Proteome Discoverer. Changes in protein abundances were considered significant with a *p* < .05 and a Log_2 difference >1.

4.11 | Accession numbers

The Arabidopsis locus identifier for *RPS6A* is At4g31700, and that for *RPS6B* is At5g10360. RNA-Seq data are deposited in NCBI-GEO under accession number GSE222967. All proteomics spectral data in this study were deposited under accession number PDX042512 at the ProteomeXchange Consortium via the MASSIVE repository (<https://massive.ucsd.edu/>).

AUTHOR CONTRIBUTIONS

Ramya Enganti, Anwesha Dasgupta, and Albrecht G. von Arnim designed the project. Ricardo A. Urquidi Camacho analyzed data on polysome loading, RNA-Sequencing, and proteomics. Ramya Enganti performed research in the early stage of the project. Anwesha Dasgupta performed research in the mid and late stages of the project. Sung Ki Cho contributed the bulk of polysome gradient experiments. Lindsey L. Tucker and John S. Torreverde assisted with experiments under the guidance of Anwesha Dasgupta. Paul E. Abraham performed the proteomics analysis. Albrecht G. von Arnim analyzed data and wrote the manuscript with input from all coauthors.

ACKNOWLEDGMENTS

We thank the staff of the Oklahoma Medical Research Foundation for RNA-Sequencing services and the Advanced Computing Facility and ISAAC of the University of Tennessee Office of Information Technology for access to high performance computing.

CONFLICT OF INTEREST STATEMENT

The authors declare that they have no conflicts of interest.

PEER REVIEW

The peer review history of this article is available in the [Supporting Information](#) for this article.

DATA AVAILABILITY STATEMENT

The data that support the findings of this study are available from the corresponding author upon reasonable request.

ORCID

Anwesha Dasgupta  <https://orcid.org/0000-0002-4356-9382>

Ricardo A. Urquidi Camacho  <https://orcid.org/0000-0002-5526-3938>

Ramya Enganti  <https://orcid.org/0000-0001-7283-1389>

Sung Ki Cho  <https://orcid.org/0000-0001-8519-047X>

Lindsey L. Tucker  <https://orcid.org/0009-0001-7809-1745>

John S. Torreverde  <https://orcid.org/0009-0009-7089-3979>

Paul E. Abraham  <https://orcid.org/0000-0003-2685-9123>

Albrecht G. von Arnim  <https://orcid.org/0000-0003-3472-3357>

REFERENCES

- Ahmad, Z., Magyar, Z., Bogre, L., & Papdi, C. (2019). Cell cycle control by the target of rapamycin signalling pathway in plants. *Journal of Experimental Botany*, 70, 2275–2284. <https://doi.org/10.1093/jxb/erz140>
- Alexa, A., and Rahnenführer, J. (2016). topGO: Enrichment analysis for gene ontology. R package version 2.26.0. <http://www.mpi-sb.mpg.de/alexa>
- Bailey-Serres, J., & Freeling, M. (1990). Hypoxic stress-induced changes in ribosomes of maize seedling roots. *Plant Physiology*, 94, 1237–1243. <https://doi.org/10.1104/pp.94.3.1237>
- Bernstein, K. A., Gallagher, J. E., Mitchell, B. M., Granneman, S., & Baserga, S. J. (2004). The small-subunit processome is a ribosome assembly intermediate. *Eukaryotic Cell*, 3, 1619–1626. <https://doi.org/10.1128/EC.3.6.1619-1626.2004>



- Boex-Fontvieille, E., Daventure, M., Jossier, M., Zivy, M., Hodges, M., & Tcherkez, G. (2013). Photosynthetic control of Arabidopsis leaf cytoplasmic translation initiation by protein phosphorylation. *PLoS ONE*, 8, e70692. <https://doi.org/10.1371/journal.pone.0070692>
- Bohlen, J., Roiuk, M., & Teleman, A. A. (2021). Phosphorylation of ribosomal protein S6 differentially affects mRNA translation based on ORF length. *Nucleic Acids Research*, 49, 13062–13074. <https://doi.org/10.1093/nar/gkab1157>
- Chauvin, C., Koka, V., Nouschi, A., Mieulet, V., Hoareau-Aveilla, C., Dreazen, A., Cagnard, N., Carpentier, W., Kiss, T., Meyuhas, O., & Pende, M. (2014). Ribosomal protein S6 kinase activity controls the ribosome biogenesis transcriptional program. *Oncogene*, 33, 474–483. <https://doi.org/10.1038/onc.2012.606>
- Chen, G. H., Liu, M. J., Xiong, Y., Sheen, J., & Wu, S. H. (2018). TOR and RPS6 transmit light signals to enhance protein translation in deetiolating Arabidopsis seedlings. *Proceedings of the National Academy of Sciences of the United States of America*, 115, 12823–12828. <https://doi.org/10.1073/pnas.1809526115>
- Choudhary, M. K., Nomura, Y., Wang, L., Nakagami, H., & Somers, D. E. (2015). Quantitative circadian phosphoproteomic analysis of Arabidopsis reveals extensive clock control of key components in physiological, metabolic, and signaling pathways. *Molecular & Cellular Proteomics*, 14, 2243–2260. <https://doi.org/10.1074/mcp.M114.047183>
- Creff, A., Sormani, R., & Desnos, T. (2010). The two Arabidopsis RPS6 genes, encoding for cytoplasmic ribosomal proteins S6, are functionally equivalent. *Plant Molecular Biology*, 73, 533–546. <https://doi.org/10.1007/s11103-010-9639-y>
- Dobin, A., Davis, C. A., Schlesinger, F., Drenkow, J., Zaleski, C., Jha, S., Batut, P., Chaisson, M., & Gingeras, T. R. (2013). STAR: Ultrafast universal RNA-seq aligner. *Bioinformatics*, 29, 15–21. <https://doi.org/10.1093/bioinformatics/bts635>
- Dobrenel, T., Mancera-Martinez, E., Forzani, C., Azzopardi, M., Davature, M., Moreau, M., Schepetilnikov, M., Chicher, J., Langella, O., Zivy, M., Robaglia, C., Ryabova, L. A., Hanson, J., & Meyer, C. (2016). The Arabidopsis TOR kinase specifically regulates the expression of nuclear genes coding for plastidic ribosomal proteins and the phosphorylation of the cytosolic ribosomal protein S6. *Frontiers in Plant Science*, 7, 1611. <https://doi.org/10.3389/fpls.2016.01611>
- Dorfer, V., Pichler, P., Stranzl, T., Stadlmann, J., Taus, T., Winkler, S., & Mechtler, K. (2014). MS Amanda, a universal identification algorithm optimized for high accuracy tandem mass spectra. *Journal of Proteome Research*, 13, 3679–3684. <https://doi.org/10.1021/pr500202e>
- Duncan, R., & McConkey, E. H. (1982). Preferential utilization of phosphorylated 40-S ribosomal subunits during initiation complex formation. *European Journal of Biochemistry*, 123, 535–538. <https://doi.org/10.1111/j.1432-1033.1982.tb06564.x>
- Enganti, R., Cho, S. K., Toperzer, J. D., Urquidi-Camacho, R. A., Cakir, O. S., Ray, A. P., Abraham, P. E., Hettich, R. L., & von Arnim, A. G. (2018). Phosphorylation of ribosomal protein RPS6 integrates light signals and circadian clock signals. *Frontiers in Plant Science*, 8, 2210. <https://doi.org/10.3389/fpls.2017.02210>
- Gressner, A. M., & Wool, I. G. (1974). The phosphorylation of liver ribosomal proteins in vivo. Evidence that only a single small subunit protein (S6) is phosphorylated. *The Journal of Biological Chemistry*, 249, 6917–6925. [https://doi.org/10.1016/S0021-9258\(19\)42145-5](https://doi.org/10.1016/S0021-9258(19)42145-5)
- Huber, W., Carey, V. J., Gentleman, R., Anders, S., Carlson, M., Carvalho, B. S., Bravo, H. C., Davis, S., Gatto, L., Girke, T., Gottardo, R., Hahne, F., Hansen, K. D., Irizarry, R. A., Lawrence, M., Love, M. I., MacDonald, J., Obenchain, V., Oles, A. K., ... Morgan, M. (2015). Orchestrating high-throughput genomic analysis with Bioconductor. *Nature Methods*, 12, 115–121. <https://doi.org/10.1038/nmeth.3252>
- Ingargiola, C., Jehanno, I., Forzani, C., Marmagne, A., Broutin, J., Clement, G., Leprince, A. S., & Meyer, C. (2023). The Arabidopsis target of rapamycin (TOR) kinase regulates ammonium assimilation and glutamine metabolism. *Plant Physiology*, 192, 2943–2957. <https://doi.org/10.1093/plphys/kiad216>
- Kabat, D. (1970). Phosphorylation of ribosomal proteins in rabbit reticulocytes. *Characterization and Regulatory Aspects. Biochemistry*, 9, 4160–4175. <https://doi.org/10.1021/bi00823a019>
- Käll, L., Canterbury, J. D., Weston, J., Noble, W. S., & MacCoss, M. J. (2007). Semi-supervised learning for peptide identification from shotgun proteomics datasets. *Nature Methods*, 4, 923–925. <https://doi.org/10.1038/nmeth1113>
- Khalailah, A., Dreazen, A., Kahtib, A., Apel, R., Swisa, A., Kidess-Bassir, N., Maitra, A., Meyuhas, O., Dor, Y., & Zamir, G. (2013). Phosphorylation of ribosomal protein S6 attenuates DNA damage and tumor suppression during development of pancreatic cancer. *Cancer Research*, 73, 1811–1820. <https://doi.org/10.1158/0008-5472.CAN-12-2014>
- Kim, B. H., Cai, X., Vaughn, J. N., & von Arnim, A. G. (2007). On the functions of the h subunit of eukaryotic initiation factor 3 in late stages of translation initiation. *Genome Biology*, 8, R60. <https://doi.org/10.1186/gb-2007-8-4-r60>
- Kleinboelting, N., Huep, G., Kloetgen, A., Viehoveer, P., & Weisshaar, B. (2012). GABI-Kat SimpleSearch: New features of the Arabidopsis thaliana T-DNA mutant database. *Nucleic Acids Research*, 40, D1211–D1215. <https://doi.org/10.1093/nar/gkr1047>
- Knight, Z. A., Tan, K., Birsoy, K., Schmidt, S., Garrison, J. L., Wysocki, R. W., Emiliano, A., Ekstrand, M. I., & Friedman, J. M. (2012). Molecular profiling of activated neurons by phosphorylated ribosome capture. *Cell*, 151, 1126–1137. <https://doi.org/10.1016/j.cell.2012.10.039>
- Liao, Y., Smyth, G. K., & Shi, W. (2014). featureCounts: An efficient general purpose program for assigning sequence reads to genomic features. *Bioinformatics*, 30, 923–930. <https://doi.org/10.1093/bioinformatics/btt656>
- Liu, M. J., Wu, S. H., & Chen, H. M. (2012). Widespread translational control contributes to the regulation of Arabidopsis photomorphogenesis. *Molecular Systems Biology*, 8, 566. <https://doi.org/10.1038/msb.2011.97>
- Lokdarshi, A., Guan, J., Urquidi Camacho, R. A., Cho, S. K., Morgan, P. W., Leonard, M., Shimono, M., Day, B., & von Arnim, A. G. (2020). Light activates the translational regulatory kinase GCN2 via reactive oxygen species emanating from the chloroplast. *Plant Cell*, 32, 1161–1178. <https://doi.org/10.1105/tpc.19.00751>
- Lokdarshi, A., Morgan, P. W., Franks, M., Emert, Z., Emanuel, C., & von Arnim, A. G. (2020). Light-dependent activation of the GCN2 kinase under cold and salt stress is mediated by the photosynthetic status of the chloroplast. *Frontiers in Plant Science*, 11, 431. <https://doi.org/10.3389/fpls.2020.00431>
- Love, M. I., Huber, W., & Anders, S. (2014). Moderated estimation of fold change and dispersion for RNA-seq data with DESeq2. *Genome Biology*, 15, 550. <https://doi.org/10.1186/s13059-014-0550-8>
- Mahfouz, M. M., Kim, S., Delauney, A. J., & Verma, D. P. (2006). Arabidopsis TARGET OF RAPAMYCIN interacts with RAPTOR, which regulates the activity of S6 kinase in response to osmotic stress signals. *Plant Cell*, 18, 477–490. <https://doi.org/10.1105/tpc.105.035931>
- Mancera-Martinez, E., Dong, Y., Makarian, J., Srour, O., Thiebauld, O., Jamsheer, M., Chicher, J., Hammann, P., Schepetilnikov, M., & Ryabova, L. A. (2021). Phosphorylation of a reinitiation supporting protein, RISP, determines its function in translation reinitiation. *Nucleic Acids Research*, 49, 6908–6924. <https://doi.org/10.1093/nar/gkab501>
- Margalha, L., Confraria, A., & Baena-Gonzalez, E. (2019). SnRK1 and TOR: Modulating growth-defense trade-offs in plant stress responses. *Journal of Experimental Botany*, 70, 2261–2274. <https://doi.org/10.1093/jxb/erz066>



- Mergner, J., Frejno, M., Messerer, M., Lang, D., Samaras, P., Wilhelm, M., Mayer, K. F. X., Schwechheimer, C., & Kuster, B. (2020). Proteomic and transcriptomic profiling of aerial organ development in *Arabidopsis*. *Sci Data*, 7, 334. <https://doi.org/10.1038/s41597-020-00678-w>
- Meyuhas, O. (2008). Physiological roles of ribosomal protein S6: One of its kind. *International Review of Cell and Molecular Biology*, 268, 1–37. [https://doi.org/10.1016/S1937-6448\(08\)00801-0](https://doi.org/10.1016/S1937-6448(08)00801-0)
- Murchie, E. H., & Lawson, T. (2013). Chlorophyll fluorescence analysis: A guide to good practice and understanding some new applications. *Journal of Experimental Botany*, 64, 3983–3998. <https://doi.org/10.1093/jxb/ert208>
- Pachler, K., Karl, T., Kolmann, K., Mehlmer, N., Eder, M., Loeffler, M., Oender, K., Hochleitner, E. O., Lottspeich, F., Bresgen, N., Richter, K., Breitenbach, M., & Koller, L. (2004). Functional interaction in establishment of ribosomal integrity between small subunit protein rpS6 and translational regulator rPL10/Grc5p. *FEMS Yeast Research*, 5, 271–280. <https://doi.org/10.1016/j.femsyr.2004.07.009>
- Panchy, N., von Arnim, A. G., & Hong, T. (2020). Early detection of day-lengths with a feedforward circuit coregulated by circadian and diurnal cycles. *Biophysical Journal*, 119, 1878–1895. <https://doi.org/10.1016/j.bpj.2020.09.025>
- Puighermanal, E., Biever, A., Pascoli, V., Melser, S., Pratlong, M., Cutando, L., Rialle, S., Severac, D., Boubaker-Vitre, J., Meyuhas, O., Marsicano, G., Luscher, C., & Valjent, E. (2017). Ribosomal protein S6 phosphorylation is involved in novelty-induced locomotion, synaptic plasticity and mRNA translation. *Frontiers in Molecular Neuroscience*, 10, 419. <https://doi.org/10.3389/fnmol.2017.00419>
- Ren, M., Venglat, P., Qiu, S., Feng, L., Cao, Y., Wang, E., Xiang, D., Wang, J., Alexander, D., Chalivendra, S., Logan, D., Mattoo, A., Selvaraj, G., & Datla, R. (2012). Target of rapamycin signaling regulates metabolism, growth, and life span in *Arabidopsis*. *Plant Cell*, 24, 4850–4874. <https://doi.org/10.1105/tpc.112.107144>
- Robledo, S., Idol, R. A., Crimmins, D. L., Ladenson, J. H., Mason, P. J., & Bessler, M. (2008). The role of human ribosomal proteins in the maturation of rRNA and ribosome production. *RNA*, 14, 1918–1929. <https://doi.org/10.1261/rna.1132008>
- Ruvinsky, I., Katz, M., Dreazen, A., Gielchinsky, Y., Saada, A., Freedman, N., Mishani, E., Zimmerman, G., Kasir, J., & Meyuhas, O. (2009). Mice deficient in ribosomal protein S6 phosphorylation suffer from muscle weakness that reflects a growth defect and energy deficit. *PLoS ONE*, 4, e5618. <https://doi.org/10.1371/journal.pone.0005618>
- Ruvinsky, I., Sharon, N., Lerer, T., Cohen, H., Stolovich-Rain, M., Nir, T., Dor, Y., Zisman, P., & Meyuhas, O. (2005). Ribosomal protein S6 phosphorylation is a determinant of cell size and glucose homeostasis. *Genes & Development*, 19, 2199–2211. <https://doi.org/10.1101/gad.351605>
- Scarpin, M. R., Simmons, C. H., & Brunkard, J. O. (2022). Translating across kingdoms: Target of rapamycin promotes protein synthesis through conserved and divergent pathways in plants. *Journal of Experimental Botany*, 73, 7016–7025. <https://doi.org/10.1093/jxb/erac267>
- Scharf, K. D., & Nover, L. (1982). Heat-shock-induced alterations of ribosomal protein phosphorylation in plant cell cultures. *Cell*, 30, 427–437. [https://doi.org/10.1016/0092-8674\(82\)90240-9](https://doi.org/10.1016/0092-8674(82)90240-9)
- Schepetilnikov, M., Dimitrova, M., Mancera-Martinez, E., Geldreich, A., Keller, M., & Ryabova, L. A. (2013). TOR and S6K1 promote translation reinitiation of uORF-containing mRNAs via phosphorylation of eIF3h. *The EMBO Journal*, 32, 1087–1102. <https://doi.org/10.1038/emboj.2013.61>
- Stephens, M. (2017). False discovery rates: A new deal. *Biostatistics*, 18, 275–294. <https://doi.org/10.1093/biostatistics/kxw041>
- Turkina, M. V., Klang Arstrand, H., & Vener, A. V. (2011). Differential phosphorylation of ribosomal proteins in *Arabidopsis thaliana* plants during day and night. *PLoS ONE*, 6, e29307. <https://doi.org/10.1371/journal.pone.0029307>
- Van Lijsebettens, M., Vanderhaeghen, R., De Block, M., Bauw, G., Villarroel, R., & Van Montagu, M. (1994). An S18 ribosomal protein gene copy at the *Arabidopsis* PFL locus affects plant development by its specific expression in meristems. *The EMBO Journal*, 13, 3378–3388. <https://doi.org/10.1002/j.1460-2075.1994.tb06640.x>
- Wang, L., Wang, S., & Li, W. (2012). RSeQC: Quality control of RNA-seq experiments. *Bioinformatics*, 28, 2184–2185. <https://doi.org/10.1093/bioinformatics/bts356>
- Williams, A. J., Werner-Fraczek, J., Chang, I., & Bailey-Serres, J. (2003). Regulated phosphorylation of 40S ribosomal protein S6 in root tips of maize. *Plant Physiology*, 132, 2086–2097. <https://doi.org/10.1104/pp.103.022749>
- Wittenberg, A. D., Azar, S., Klochendler, A., Stolovich-Rain, M., Avraham, S., Birnbaum, L., Binder Gallimidi, A., Katz, M., Dor, Y., & Meyuhas, O. (2016). Phosphorylated ribosomal protein S6 is required for Akt-driven hyperplasia and malignant transformation, but not for hypertrophy, aneuploidy and hyperfunction of pancreatic beta-cells. *PLoS ONE*, 11, e0149995. <https://doi.org/10.1371/journal.pone.0149995>
- Yakovleva, A., & Kulaeva, O. N. (1987). The effect of phytohormones on phosphorylation of ribosomal proteins in detached pumpkin cotyledons. *Biochemie und Physiologie der Pflanzen*, 182, 359–365. [https://doi.org/10.1016/S0015-3796\(87\)80002-1](https://doi.org/10.1016/S0015-3796(87)80002-1)
- Yerlikaya, S., Meusburger, M., Kumari, R., Huber, A., Anrather, D., Costanzo, M., Boone, C., Ammerer, G., Baranov, P. V., & Loewith, R. (2016). TORC1 and TORC2 work together to regulate ribosomal protein S6 phosphorylation in *Saccharomyces cerevisiae*. *Molecular Biology of the Cell*, 27, 397–409. <https://doi.org/10.1091/mbc.e15-08-0594>

SUPPORTING INFORMATION

Additional supporting information can be found online in the Supporting Information section at the end of this article.

How to cite this article: Dasgupta, A., Urquidi Camacho, R. A., Enganti, R., Cho, S. K., Tucker, L. L., Torreverde, J. S., Abraham, P. E., & von Arnim, A. G. (2024). A phosphorylation-deficient ribosomal protein eS6 is largely functional in *Arabidopsis thaliana*, rescuing mutant defects from global translation and gene expression to photosynthesis and growth. *Plant Direct*, 8(1), e566. <https://doi.org/10.1002/pld3.566>